Collapse of Thermoresponsive Brushes and the Tuning of Protein Adsorption

2 AUTHORS:

Avraham Halperin
French National Centre for Scientific Research
119 PUBLICATIONS **3,900** CITATIONS

SEE PROFILE

Martin Kröger
ETH Zurich
239 PUBLICATIONS **3,828** CITATIONS

SEE PROFILE

# Collapse of Thermoresponsive Brushes and the Tuning of Protein Adsorption

A. Halperin*,† and M. Kröger*,‡

†University of Grenoble 1/CNRS, LIPhy UMR 5588, BP 87, 38041 Grenoble, France

‡Polymer Physics, ETH Zurich, Wolfgang-Pauli-Strasse 10, CH-8093 Zurich, Switzerland

ABSTRACT: Protein adsorption onto brush displaying surfaces is strongly affected by collapse, an effect utilized in protein chromatography and in harvesting cell sheets for tissue engineering applications. For relatively small particles, the free energy penalty incurred upon insertion into the brush F_{ins} is related to the work expended against the osmotic pressure of the unperturbed brush. Within the self-consistent field (SCF) theory of brushes, the scale of F_{ins} decreases with the brush thickness $\langle z \rangle$ because the value of the osmotic pressure at the grafting surface $\Pi(0) \sim \langle z \rangle$ irrespective of the interaction free energy. Brush collapse thus favors adsorption because it reduces F_{ins} via two effects: (i) lowering of the osmotic pressure and (ii) a possible decrease of the inserted volume of the particle. These general results are supplemented by numerical solutions of SCF equations for the collapse of thermo-responsive poly(N-isopropylacrylamide) (PNIPAM) brushes as described by the empirical free energy of Afroze et al. (*J. Mol. Struct.* **2000**, *554*, 55). These yield the monomer concentration profiles $c(z)$ and the corresponding osmotic pressure profiles $\Pi(z)$ as functions of the altitude z and the temperature T. $c(z)$ and $\Pi(z)$ are then used to characterize F_{ins} for collapsed and swollen brushes as well as the adsorption isotherms for three adsorption mechanisms of relevance to *ex vivo* biotechnology applications involving PNIPAM brushes: (a) primary adsorption at the wall, (b) adsorption onto a ligand embedded within the brush, and (c) ternary adsorption within the brush due to weak attraction between the polymer and the adsorbing particle. Our results rationalize existing experimental results concerning the interactions between proteins and PNIPAM brushes and predict the effects of tuning parameters such as grafting density, polymerization degree and protein dimensions.
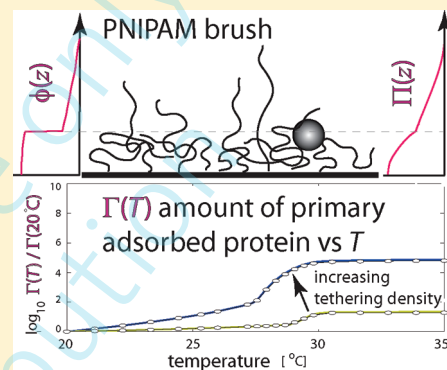
I. INTRODUCTION

Brushes of neutral water-soluble polymers (NWSP) allow to tune protein adsorption and cellular adhesion. The two principal applications involved are epitomized by brushes of poly(ethylene glycol) (PEG) and of poly(N-isopropylacrylamide) (PNIPAM). Water swollen PEG brushes are deployed to repress protein adsorption and cellular adhesion.[1−3] In contrast, thermoresponsive PNIPAM brushes enables switching between repulsive and attractive states.[4] Collapsed PNIPAM brushes, above the lower critical solution temperature (LCST) of PNIPAM, adsorb proteins and favor cell adhesion while swollen brushes, below the LCST, exhibit the opposite trend. This last feature led to applications in protein separations[5−7] and harvesting of cell sheets for tissue engineering.[8−11] The steadily growing activity in the area established the utility of such thermoresponsive brushes while raising questions about design parameters and mechanisms of function.[4,11] The exploration of these issues calls for a theoretical framework relating the multiple parameters involved: Σ, the area per grafted chain, N, its polymerization degree, T, the temperature, the geometry and dimensions of the adsorbed proteins etc. The formulation of such theory is however hampered by uncertainties concerning the physical chemistry of PNIPAM: its precise phase diagram, the corresponding interaction free energy density, $k_B T f_{int}$, and the values of molecular

parameters such as the persistence length, l_p (Appendix A). With these difficulties in mind we explore an equilibrium theory of adsorption of neutral colloidal particles onto surfaces displaying thermoresponsive NWSP brushes exemplified by PNIPAM. Our discussion emphasizes the effect of collapse associated with LCST. It utilizes analytical self-consistent field (SCF) theory of neutral brushes[12−14] and yields Langmuir type adsorption isotherms and their dependence on Σ, N, T, as well as the particle dimensions. To circumvent the difficulties noted earlier our analysis pursues two directions. In one we consider an arbitrary f_{int} and derive general and simple analytical results on the effect of collapse. In the second we perform complementary numerical SCF calculations utilizing an empirical f_{int} of PNIPAM solutions proposed by Afroze et al.[15] (Appendix A). This f_{int} is used because it is in qualitative agreement with experimental results concerning the structure of PNIPAM brushes.[16,17] To highlight the distinctive features of this description we contrast the numerical results with those obtained for "classical" brushes (Appendix A). Within our theory the insertion of a particle into the brush incurs a free energy penalty, F_{ins}, due to the work

expended against the osmotic pressure of the brush. The leading effects of brush collapse are due to the reduction of the osmotic pressure within the brush and the associated decrease in F_{ins}. In certain cases F_{ins} is reduced further because the lowering of the brush height upon collapse decreases the inserted volume of the particle. The reduction of F_{ins} favors adsorption onto collapsed brushes in general. For the case of PNIPAM brushes as described by f_{int} of Afroze et al. (Appendix A), it predicts enhanced protein adsorption upon increasing T to above $T \simeq 29$ °C. These results account for the observed trends concerning protein adsorption onto PNIPAM brushes. They are of relevance to harvesting of cell sheets to the extent that adsorption of adhesion proteins is involved.

The formulation of our theory involves four elements characterizing the brush−particles interactions: the adsorbing particles, the mode of particle entry into the brush, the brush structure, and the adsorption mechanism. The adsorbing moieties, proteins or colloidal particles, are modeled as neutral and impenetrable particles interacting via hard core potentials. These are characterized by two types of attributes. One set concerns their geometry and includes their volume, surface area, dimensions etc. The second set concerns their interactions with the grafting surface and the polymer chains as characterized by phenomenological interaction energies. Regarding the particle entry into the brush we focus on the insertion mode where a particle placed inside the brush induces only short ranged perturbation of the concentration profile.[18−25] This implies two requirements: (i) The particle−monomer interactions should not produce a dense monomer layer surrounding the particle. Accordingly, nonspecific interactions should be repulsive or weakly attractive. There is no limitation on specific interactions involving binding sites. (ii) The insertion of the particle should not induce compression of the brush. In physical terms, the chains' trajectories should be able to circumvent the particle. For brushes of long chains this condition is fulfilled for typical globular proteins and for proteins incorporating cylindrical domains such as adhesion proteins. In such cases F_{ins} reflects the work expended against the osmotic pressure within the *unperturbed* brush, $\Pi(z)$.[19,21,23−25] $\Pi(z)$ varies with the altitude z and the local monomer concentration profile $c(z)$ or the monomer volume fraction $\phi(z) = c(z)a^3$ of monomers of size a. As we shall elaborate later $\Pi(z)$ is identical to the osmotic pressure in a uniform bulk solution with $\phi = \phi(z)$ and

$$F_{ins}(z) = \int_0^h \Pi(z') A_{prt}(z, z')\, \mathrm{d}z' \tag{1}$$

where $A_{prt}(z, z')\, \mathrm{d}z$ is the cross sectional volume at z' of a particle whose geometrical center is at altitude z, and h is the brush height to be determined within the SCF theory. F_{ins} as specified by eq 1 is an assumption supported by simulations[18,22,25] and their analysis[24,34] as well as by arguments based on the Alexander model[24] (Appendix B).

To fully implement this approach it is first necessary to determine the T dependent $\phi(z)$ and the corresponding $\Pi(z)$. This brings us to the next ingredient of our analysis, namely the description of the brush. Here we first emphasize that while neutral brushes swollen by good solvents exhibit an effectively unique behavior, brush collapse may involve qualitatively different $\phi(z)$ and $\Pi(z)$. These differences are traceable to the interaction free energy density, $k_B T f_{int}$, of the bare, particle-free brush. It is especially useful to distinguish between two cases

(Appendix A): One concerns "classical" brushes where f_{int} is dominated by binary and ternary monomer−monomer interactions.[13] Only the second virial coefficient can change sign while higher order interactions are purely repulsive.[26,27] In this familiar scenario collapse occurs upon lowering T and a LCST does not occur. In addition, the monomer concentration profiles, as obtained from SCF theory, exhibits a jump at the outer edge of the collapsed brush.[13] In contrast, different virial coefficients can change sign in f_{int} of "non-classical" brushes thus allowing for LCST behavior and for vertical phase separation within the brush. In turn, this last feature involves a SCF $\phi(z)$ exhibiting a discontinuity within the brush z range.[28−32] The collapse behavior of classical brushes is realized in nonaqueous solvents[33] while evidence suggests that PNIPAM brushes in water exhibit nonclassical behavior.[16,17] Our analysis accordingly focuses on the nonclassical case thus complementing an earlier discussion of the classical brush scenario.[34] Since the "classical" f_{int} was invoked in discussions of PNIPAM coils[35,36] and brushes[37,38] we compare the numerical results of the two scenarios. Note that the properties of the solvent are incorporated into the mixing free energy of the polymer and are thus manifested in the virial coefficients. In this context it is helpful to underline the differences between brushes of PEG and PNIPAM because both are utilized in biotechnology applications at near ambient T. Ambient T is far removed from the LCST of PEG, $T_c \approx 100$ °C. The theory of PEG brushes and their interactions with proteins invokes thus a "classical" f_{int} justified by the behavior of aqueous solutions of PEG.[39] In contrast, the applications of thermoresponsive PNIPAM brushes utilize their collapse around the LCST at $T_c \approx 30$ °C[15,40−43] thus requiring a "nonclassical" description.

Within our model particle adsorption reflects a balance between F_{ins} penalizing insertion and an attractive free energy F_{att} favoring it. The fourth element of our discussion concerns the adsorption mechanisms that determine F_{att}. For brevity we focus on three simple scenarios (Figure 1): (i) nonspecific primary adsorption at the grafting surface due to particle-wall contact attraction,[19,44,45] (ii) specific adsorption to ligands anchored at fixed altitude within the brush,[5,6] and (iii) ternary adsorption within the brush due to weak and nonspecific monomer−particle attraction.[21,23,46,47] These include mechanisms invoked in discussions of the interactions between proteins and PEG brushes.[19,21,23,44−47] The specific choice is motivated by experimental results regarding PNIPAM-protein interactions and observations concerning three PNIPAM applications utilizing thermally induced collapse/swelling of brushes. In particular: (I) cell sheets adhering to collapsed PNIPAM brushes can be detached upon lowering the temperature to below the LCST.[8−10] Importantly, the cell detachment is associated with desorption of adhesion proteins deposited by the adhering cells.[11] (II) Proteins adsorb onto PNIPAM brushes above the LCST and desorb below the LCST thus allowing to program the adsorption and release of proteins in microfluidic devices[7] and electrodes.[48] (III) Protein chromatography based on PNIPAM brushes incorporating ligands anchored at fixed altitudes. A specific protein binds to the ligand below the LCST and desorbs above the LCST.[5,6] This last case is of special interest because the protein binds specifically to the ligand and the swelling of the PNIPAM brushes serves to release it. This is in contrast to the first two examples where the adsorption may reflect attraction to both PNIPAM chains and the underlying grafting surface.

The remainder of the article is organized as follows. The Alexander model yields a simple picture regarding the relationship
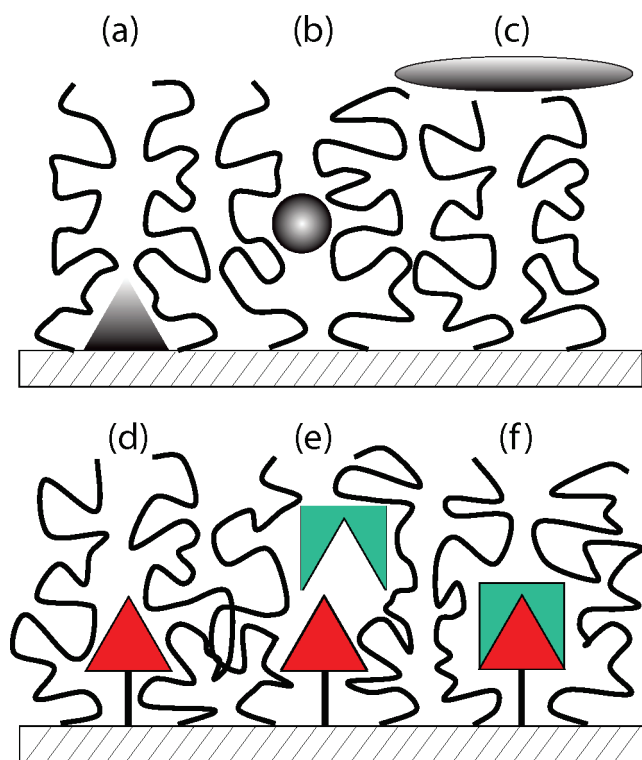
Figure 1. Three adsorption modes onto an unmodified brush: (a) primary adsorption at the wall, (b) ternary adsorption within the brush (c) secondary adsorption at the outer edge of the brush. Brushes incorporating ligands anchored via short tethers (d) exhibit an additional mode due to specific binding of certain proteins (e) to the ligands (f).

between collapse and the osmotic pressure as well as the physical origins of F_{ins}. This picture and its limitations are discussed for arbitrary f_{int} in section II. The analytical SCF theory of $\phi(z)$ and $\Pi(z)$ and their variation with T is described in section III. The discussion involves two parts: (a) model independent results concerning $\Pi(0)$ and the average $\Pi(z)$, $\overline{\Pi}$, as obtained for arbitrary f_{int}, (b) numerical results concerning $\phi(z)$ and $\Pi(z)$ of PNIPAM brushes as described by the empirical f_{int} of Afroze et al. (Appendix A2). We then utilize these results to discuss the adsorption scenarios. In particular, the effect of collapse on adsorption is analyzed in section IV focusing on primary adsorption at the wall, ligand adsorption and weak nonspecific adsorption within the brush. All numerical calculations confront results obtained for f_{int} of Afroze et al. with those based on the classical f_{int}. The Discussion presents an overview of our results, proposed experiments allowing to confront the theory as well as a summary of currently unresolved issues. In Appendix A, we summarize the necessary background concerning two issues. One is the distinction between classical and nonclassical brushes in general. The second concerns the particular case of PNIPAM and its brushes focusing on topics affecting the modeling of their interactions with proteins. These include the phase behavior of PNIPAM, the evidence for nonclassical brush behavior and the applicability of two state models, the current uncertainties concerning the monomer size a and the persistence length l_p and the interactions between PNIPAM and proteins. Technical details concerning our discussion of the Alexander model, the SCF theory and its implementation are delegated to Appendices B, C, and D respectively.

II. ON Π AND THE OSMOTIC PENALTY WITHIN THE ALEXANDER MODEL

The main thrust of our analysis involves SCF theory. However, it is helpful to introduce the discussion of collapse, osmotic pressure and F_{ins} via the simpler Alexander model.[49] In the following we use it to present a simple analysis of the relationship between brush collapse and the osmotic pressure. We also discuss the physical origins of F_{ins}, as given by eq 1, and the underlying contributions due to the elastic and interaction free energies. The technical details on this last topic are described in Appendix B. We immediately stress that by construction the Alexander model does not allow for vertical phase separation. However, the results of the Alexander model concerning the osmotic pressure can be correctly reformulated, in a similar form, using the SCF theory. In turn, the SCF version applies to all brushes and in particular to nonclassical brushes undergoing vertical phase separation.

The Alexander model of a brush involves two assumptions: (i) a step like concentration profile with monomer volume fraction $\Phi = Na^3/\Sigma H = \text{const}'$ where Σ is the area per headgroup, H is the brush height, N is the polymerization degree and a is the monomer size; (ii) uniformly stretched chains with their free ends at the brush boundary at height H. We utilize Φ and H to avoid confusion with the SCF counterparts, $\phi(z)$ and h. The free energy per chain comprises two terms $F_{chain} = F_{int} + F_{el}$ allowing respectively for the interaction and elastic contributions. Within the mean field (MF) version of the model the chain exhibit Gaussian elasticity and $F_{el}/k_BT = 3H^2/2Npa^2 = 3N\sigma^2/2\Phi^2$ where $\sigma = a^2/\Sigma$ is the grafting density of the head-groups, and p the number of monomers in a persistent segment of length $l_p \simeq pa$. Discussions of the Alexander model often focus on the classical case with F_{int} allowing for binary and ternary monomer interactions. In distinction, here we specify F_{int} in terms of an arbitrary interaction free energy density k_BTf_{int} such that the interaction free energy per chain is $F_{int}/k_BT = \Sigma Hf_{int} = Na^3f_{int}/\Phi$. The equilibrium condition $\partial F_{chain}/\Sigma \partial H = 0$ leads to

$$\frac{\Pi a^3}{k_B T} = \frac{3\sigma^2}{\Phi} = \frac{3\sigma}{N}\frac{H}{pa} \tag{2}$$

where $\Pi/k_BT = \Phi \partial f_{int}/\partial \Phi - f_{int}$ is the step-like osmotic pressure corresponding to a solution of free chains with an identical Φ. Equation 2 reflects a force balance with the chain tension per unit area

$$T_n = \frac{\partial F_{el}}{\Sigma \partial H} = 3k_B T \frac{H}{\Sigma N p a^2} \tag{3}$$

Accordingly, for a brush with a given σ and N the transition from good to poor solvent conditions is characterized by

$$\frac{\Pi_p}{\Pi_g} = \frac{H_p}{H_g} \tag{4}$$

where the values of Π and H in poor and good solvent are denoted respectively by the indices p and g. Since our discussion involves an arbitrary f_{int} eq 4 is independent of the model specifying it. Note however that a vertical phase separation in the Alexander model wrongly appears as a transition between two H values[30] and eq 4 can be misleading. Yet the SCF counterpart of eq 4, as will be derived in section III, is free from such difficulties.

The Alexander model also enables an analysis of the physics underlying the insertion scenario and the associated F_{ins} and thus leading to eq 1. This discussion is of interest because the direct evidence on this subject originates from computer simulations.[18,22,24,25] The detailed analysis concerning the case of insertion into a brush of laterally immobile chains is presented in Appendix B. For fully inserted spherical particle of radius R_{prt} $\ll H$ and volume $V^0_{prt} \approx R^3_{prt}$ it leads to the Alexander model version of eq 1

$$F_{ins} = \Pi V^0_{prt} \tag{5}$$

This MF result applies to all solvent qualities. Note however that for an athermal solvent, when the MF approximation is poor, $F_{ins} = 8\Pi V^0_{prt}/7 > \Pi V^0_{prt}$.[12,24] Note also that within our analysis $F_{ins} = \Pi V^0_{prt}$ reflects the combination of two effects. The insertion of the particle increases both H and Φ thus leading to corresponding increase in F_{el} and F_{int}. Thus, while eq 5 is reminiscent of F_{ins} for bulk solutions of free chains,[50] the underlying mechanism is different because the contribution of F_{el} has no counterpart in the bulk case. Similar results were obtained for full insertion of a cylindrical particle into a brush of laterally mobile chains, when the brush structure is laterally uniform.

III. ON $\Pi(Z)$ AND F_{INS} WITHIN THE SCF THEORY

In reality, the concentration and osmotic pressure profiles vary with the altitude z. The leading features of the z dependence are captured by the analytical SCF theory we utilize. To avoid confusion with the Alexander model, in our discussion of the SCF theory we replace Φ by $\phi(z)$ and H by h. The SCF description, with z dependent $\phi(z)$ and $\Pi(z)$, is useful for a number of reasons: first of all, it allows for a vertical phase separation within the brush. In addition, the SCF $\Pi(z)$ gives rise to a shape dependent F_{ins}, as given by eq 1, thus clarifying the role of the form of the adsorbing particle. Finally the SCF $\phi(z)$ can qualitatively modify the ternary adsorption behavior when vertical phase separation is involved. In subsection (A) we introduce the key SCF equations and derive model independent results concerning $\Pi(0)$ and the average $\Pi(z)$, $\bar{\Pi}$. These relate $\Pi(0)$ and $\bar{\Pi}$ to the observable moments of $\phi(z)$ for arbitrary f_{int}. Numerical solutions of $\phi(z)$ and $\Pi(z)$ are discussed in subsection (B) where we compare the behavior of classical brushes and PNIPAM brushes as described by f_{int} of Afroze et al.. These highlight the qualitative differences between the two systems for selected Σ and N values. Software based on the algorithm described in Appendix D[51] enables such calculations for user chosen Σ, T and N.

A. $\Pi(0)$ and $\bar{\Pi}$ for Arbitrary f_{int}. The determination of $\phi(z) = c(z)a^3$ and $\Pi(z)$ within the analytical SCF theory (Appendix C) involves two steps. First, one obtains $\phi(z)$ utilizing the parabolic form of the exchange chemical potential $\mu(\phi)/k_BT = a^3\partial f_{int}(\phi)/\partial\phi$

$$\frac{\mu(\phi(z))}{k_BT} = \Lambda - \frac{3\pi^2}{8N^2pa^2}z^2 \tag{6}$$

where the Lagrange multiplier Λ and the brush height h are specified by the constraint

$$\int_0^h \phi(z) \, dz = N\sigma a \tag{7}$$

When f_{int} displays a nonconvex, unstable region, it is replaced by a tangent specified by the Maxwell equal area construction

(Appendix D). $\Pi(z)$ is then determined either from $\Pi/k_BT = \phi\partial f_{int}/\partial\phi - f_{int}$ or from the force balance ensuring the equality of $\Pi(z)$ with the average tension per unit area at z and leading to

$$\frac{\Pi(z)a^3}{k_BT} = \frac{3\pi^2}{4Npa^2}\int_z^h t\phi(t) \, dt \tag{8}$$

This procedure yields analytical solutions for asymptotic good and poor solvents as well as for $T = \Theta$ in the case of classical brushes, when only the second and third virial terms of f_{int} play a role (Appendix A). Its implementation for nonclassical brushes, when the phenomenological f_{int} involves higher order virial terms, requires numerical solutions. While there is no analytical solution for $\Pi(z)$ in the case of arbitrary f_{int}, the force balance eq 8 yields useful expressions for $\Pi(0)$ and $\bar{\Pi}$ (Appendix C). In particular, it leads to

$$\frac{\Pi(0)a^3}{k_BT} = \frac{3\pi^2}{4} \frac{\sigma}{N} \frac{\langle z \rangle}{pa} \tag{9}$$

where

$$\langle z \rangle = \frac{\int_0^h z\phi(z) \, dz}{\int_0^h \phi(z) \, dz} \tag{10}$$

Accordingly, for a brush with a fixed N and σ

$$\frac{\Pi_p(0)}{\Pi_g(0)} = \frac{\langle z \rangle_p}{\langle z \rangle_g} \tag{11}$$

Similarly the mean osmotic pressure $\bar{\Pi} = \int_0^h \Pi(z) \, dz/h$ in the brush is related to the second moment of $\phi(z)$ via

$$\frac{\bar{\Pi} a^3}{k_BT} = \frac{3\pi^2}{4} \frac{\sigma}{N} \frac{\langle z^2 \rangle}{pah} \tag{12}$$

where

$$\langle z^2 \rangle = \frac{\int_0^h z^2\phi(z) \, dz}{\int_0^h \phi(z) \, dz} \tag{13}$$

Equation 9 is the SCF counterpart of eq 4 obtained within the Alexander model. It differs from eq 4 in that $\Pi(0)$ replaces Π and $\langle z \rangle$ replaces $H/2$. However, $\Pi(0)$ as given by eq 9 in terms of the SCF $\langle z \rangle$ is well-defined when $\phi(z)$ displays a discontinuity due to a vertical phase separation. It thus avoids the unphysical jump introduced by the Alexander model for systems undergoing a second type of phase transition. Importantly, eqs 9, 11, and 12 can be implemented using experimentally measured $\langle z \rangle$ and $\langle z^2 \rangle$ even when f_{int} is unspecified. As we shall discuss later, eq 9 enables a simple analysis of the effect of collapse on adsorption at vicinity of the grafting surface. In qualitative terms, it captures the effect of collapse on $\Pi(z)$ and F_{ins} because it specifies their maximal values within the SCF theory.

B. $\phi(z)$ and $\Pi(z)$: Classical vs PNIPAM Brushes. Having characterized $\Pi(0)$ and $\bar{\Pi}$ for arbitrary f_{int} we now compare $\phi(z)$ and $\Pi(z)$ for two f_{int} of interest: the familiar classical case with $f_{int}a^3 = \hat{v}\phi^2 + \hat{w}\phi^3$ and $\hat{v} = 1 - \Theta/T$ and the PNIPAM f_{int} proposed by Afroze et al. (Appendix A2). The comparison involves plots of numerical results because f_{int} of Afroze et al. does not permit an analytical solution and because the classical
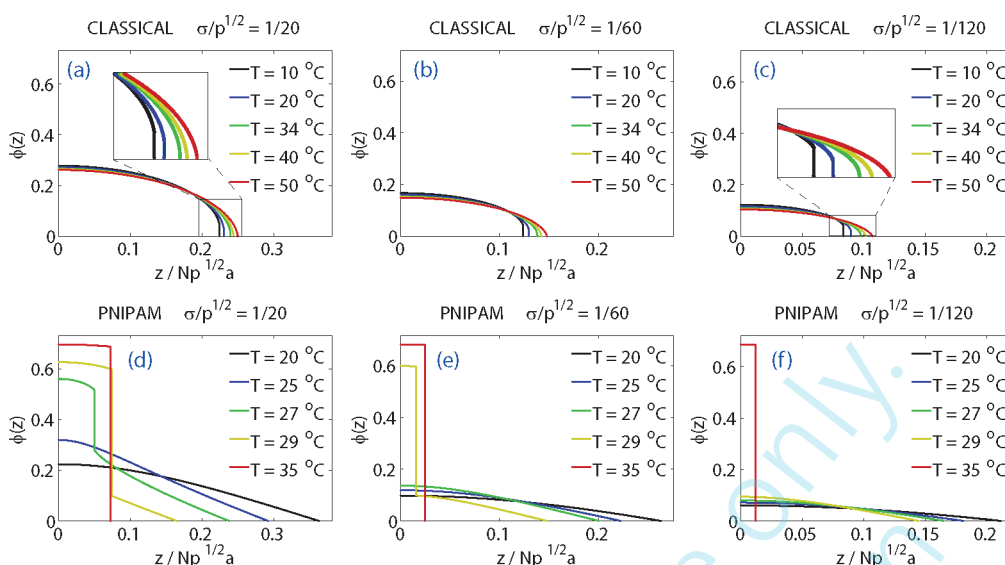
Figure 2. $\phi(z)$ vs $z/Np^{1/2}a$ profiles of (a−c) classical ($\Theta = 34\,^\circ\text{C}$) and (d−f) PNIPAM brushes at different T and surface density $\sigma/p^{1/2}$. The results are independent of the choice of a, p, and N (Appendix D). The PNIPAM profiles are distinguished by pronounced discontinuities and a wider ϕ range.
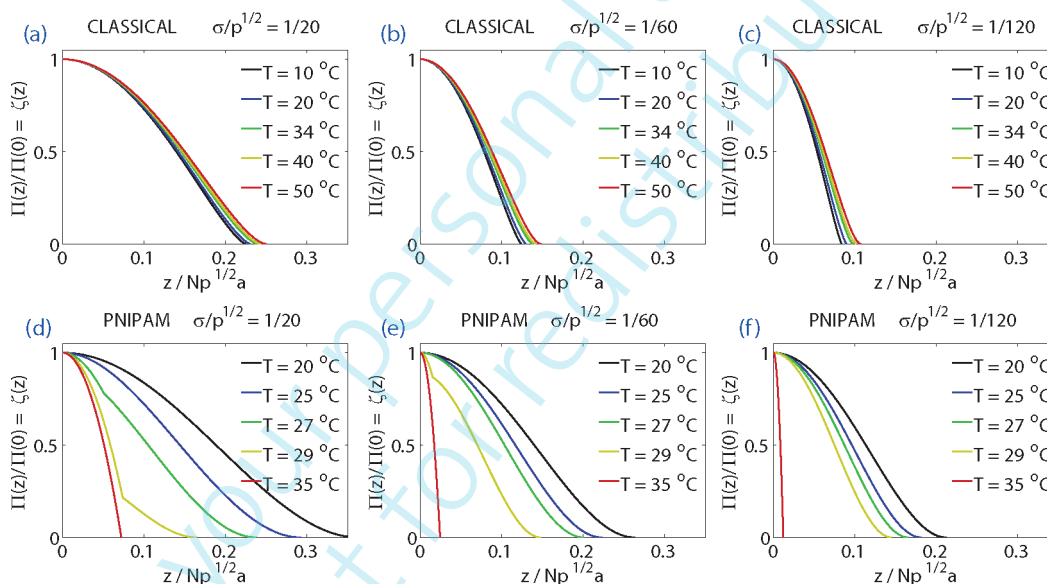

Figure 3. $\Pi(z)/\Pi(0) \equiv \zeta(z)$ vs $z/Np^{1/2}a$ profiles of (a−c) classical ($\Theta = 34\,^\circ\text{C}$) and (d−f) PNIPAM brushes at different T and $\sigma/p^{1/2}$. The results are independent of the choice of a, p, and N. The PNIPAM profiles exhibit discontinuities in slope, reflecting a vertical phase separation, and a wider z range.

f_{int} yields closed form expressions only for asymptotic cases and Θ solvents.[13] Our plots utilize reduced variables for the altitude, $z/Np^{1/2}a$, and the surface density, $\sigma/p^{1/2}$, to eliminate dependence on p, a, and N.[34] This serves to circumvent the uncertainties concerning the p and a values of PNIPAM.

In both systems brushes undergo collapse associated with an increase in density: $\langle z \rangle$ and h decrease while $\phi(0)$ increases. Yet classical and PNIPAM brushes differ in a number of points: (a) Collapse of classical systems is attained upon decreasing T while for PNIPAM brushes it is associated with an increase of T (Figure 2). Also, for PNIPAM the change from strongly swollen to fully collapse occurs over a 20 °C interval. In contrast, classical brushes undergo a small change in this range; (b) In agreement with experimental results[16,17] the SCF $\phi(z)$ profiles of PNIPAM exhibit a discontinuity reflecting a vertical phase separation. In contrast $\phi(z)$ of classical brushes are continuous and poor solvent behavior is associated with a jump at the peripheral edge of the brush i.e., $\phi(h) > 0$ instead of $\phi(h) = 0$ obtained in Θ and good solvents; (c) The $\Pi(z)$ profiles in both systems are continuous and do not cross each other. In both cases $\Pi(z)$ decreases with the T dependent solvent quality as characterized by $\langle z \rangle$ or h (Figure 3). However, $\Pi(0)$ of classical brushes increases with increasing T while for PNIPAM in the 20 °C $\leq$ $T \leq$ 40 °C range the trend is inverted (Figure 4). This feature is traceable to the T dependence of the corresponding bulk solution osmotic pressure (Appendix A). Furthermore, in contrast to the smooth $\Pi(z)$ profiles of classical brushes, PNIPAM brushes exhibit a discontinuity in the slope of $\Pi(z)$ at z_{co} corresponding
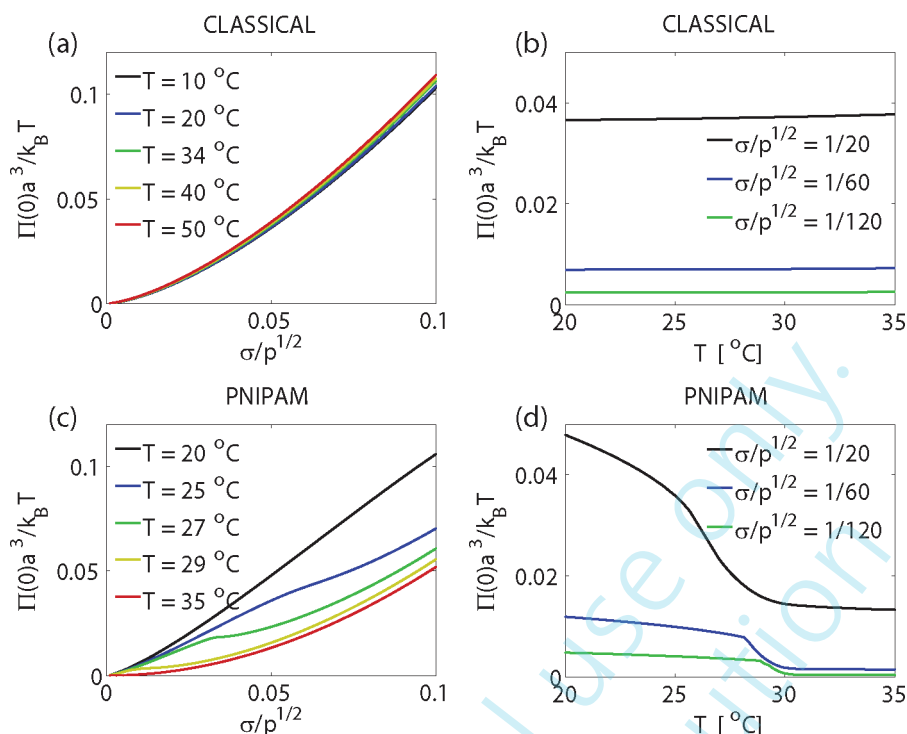
Figure 4. (a, c) $\Pi(0)a^3/k_B T$ vs $\sigma/p^{1/2}$ at different T and (b, d) $\Pi(0)a^3/k_B T$ vs T at different $\sigma/p^{1/2}$ for (a,b) classical ($\Theta = 34$ °C) and (c, d) PNIPAM brushes. In contrast to PNIPAM brushes, the classical $\Pi(0)$ increases weakly with increasing T and exhibits smooth variation with $\sigma/p^{1/2}$. The results are independent of the choice of a, p, and N.

to the coexistence associated with the vertical phase separation; (d) The vertical phase separation in PNIPAM brushes strongly affects $\langle z \rangle$.[30,31] In classical brushes the plots of $\langle z \rangle / N p^{1/2} a$ vs $\sigma/p^{1/2}$ and vs T are monotonic and continuous with a gradual change of slope (Figures 5 and 6). In contrast, the $\langle z \rangle / N p^{1/2} a$ vs $\sigma/p^{1/2}$ plots of PNIPAM in the 20 °C $\leq T \leq$ 35 °C range exhibit a horizontal S like form with both a maximum and a minimum (Figure 5). Consequently $\langle z \rangle_{20\ °C} / \langle z \rangle_T$ vs $\sigma/p^{1/2}$ exhibit a maximum for T near the LCST of PNIPAM. Similar effect was noted by Mendez et al.[52] who reported an N dependent maximum in $\langle z \rangle_{20\ °C} / \langle z \rangle_{40\ °C}$ vs $\sigma/p^{1/2}$. In distinction, our SCF results reveal a N independent maximum in $\langle z \rangle_{20\ °C} / \langle z \rangle_T$ vs $\sigma/p^{1/2}$ at $T \simeq 28$ °C and monotonically decreasing $\langle z \rangle_{20\ °C} / \langle z \rangle_{40\ °C}$ vs $\sigma/p^{1/2}$ (Figure 7). The difference occurs because f_{int} utilized in our analysis corresponds to the $N \to \infty$ limit since grafted chains have no translational entropy. The maximum in $\langle z \rangle_{20\ °C} / \langle z \rangle_T$ vs $\sigma/p^{1/2}$ leads to a corresponding effect on the adsorption isotherms. While the $\langle z \rangle / N p^{1/2} a$ vs T plots of PNIPAM are monotonic their slope can vary sharply (Figure 6). In contrast, the corresponding classical curves are weakly sloped straight lines. These features also manifest themselves in the corresponding $\Pi(0)$ plots (Figure 4). In spite of these qualitative differences, both systems follow eq 9 (Figure 8). The plots described above as well as other plots reported below can be generated for user specified parameters using our free software.[51]

IV. THE EFFECT OF BRUSH COLLAPSE ON ADSORPTION ISOTHERMS

In the following we analyze the effect of brush collapse on the adsorption of colloidal particles. Our discussion is motivated by

results concerning protein adsorption onto thermoresponsive PNIPAM brushes. The mechanisms invoked draw however on earlier work aimed at the interactions of proteins with swollen NWSP brushes exemplified by PEG (Figure 1). They differ in the nature of the attractive term, F_{att}, since in every case the adsorption is opposed by the osmotic insertion penalty, F_{ins}. The previously proposed mechanisms include: (i) primary adsorption at the grafting surface due to protein-wall attraction;[19,44−46] (ii) secondary adsorption at the exterior edge of the brush arising because of van der Waals attraction between the protein and the surface;[19] (iii) ternary adsorption, within the brush itself, due to attractive interactions between the polymer and the protein. This last scenario can assume different forms depending on the mode of attraction: (a) weak adsorption resulting from weak nonspecific attractions between the monomers and the surface of the protein;[21,23,46,47] (b) strong terminal adsorption due to binding of chain ends at specific sites;[23] (c) strong backbone adsorption arising from binding of interior chain segments to specific protein sites.[23] Other scenarios may well exist, and the relative importance of the different adsorption modes is yet to be determined.

Our discussion will focus on three scenarios chosen on the basis of the following considerations. We will not discuss secondary adsorption because it is expected to play a role only for long cylindrical particles[19] and has not been observed thus far. Strong specific ternary adsorption is important when antibodies are involved,[23] as is the case for *in vivo* applications confronting the immune system. However, the PNIPAM applications motivating our work are *ex vivo* and do not involve antibodies to the polymer. Yet, there is evidence for attractive interactions between PNIPAM and proteins, as discussed in Appendix A. The nature of these interactions is yet to be established. One may, for example
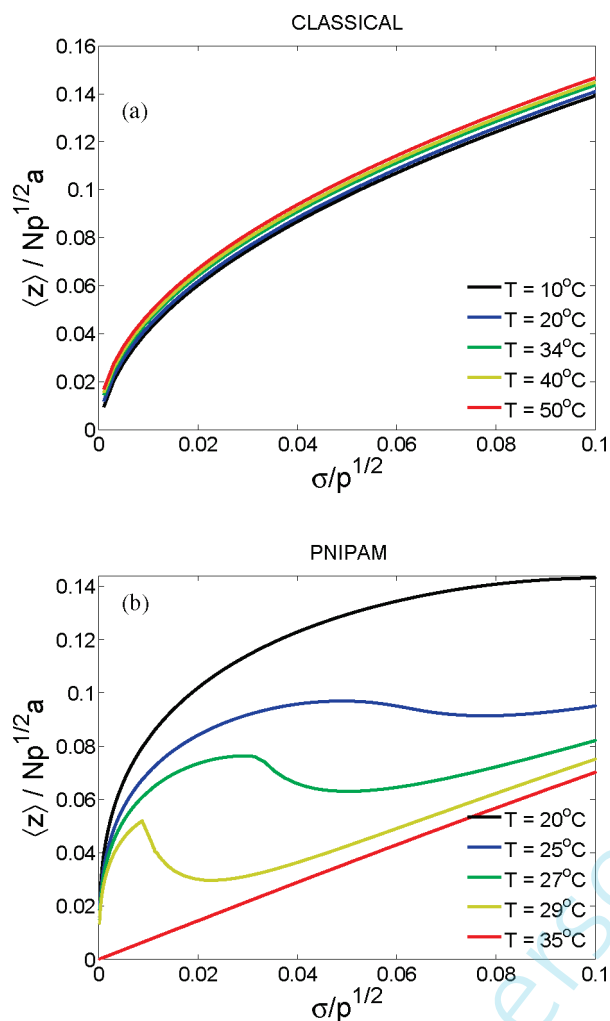
Figure 5. $\langle z \rangle / N p^{1/2} a$ vs $\sigma / p^{1/2}$ plots for (a) classical ($\Theta = 34\ ^\circ\text{C}$) and (b) PNIPAM brushes at different T. In contrast to PNIPAM the classical $\phi(z)$ profiles increase with T monotonically and at narrow range. The results are independent of the choice of a, p and N.

Figure 6. $\langle z \rangle / p^{1/2} a$ vs T plots for (a) classical ($\Theta = 34\ ^\circ\text{C}$) and (b) PNIPAM brushes at different $\sigma / p^{1/2}$. The inset in panel (a) shows the same data vs $\tau = 1 - \Theta/T$ to bring out the similarity to experimental results.[33] The classical plots are weakly increasing with T in contrast to the PNIPAM plots that also exhibit strong changes in slope associated with a vertical phase separation. The results are independent of the choice of a, p, and N.

consider specific protein sites, similar to those binding small ligands to Human Serum Albumin.[53,54] In the absence of experimental data we will invoke, for simplicity, the weak ternary adsorption model i.e., assuming particles with uniform surfaces such that a monomer in grazing contact experiences an attraction free energy $-\varepsilon k_B T$. However, in contrast to the PEG-protein systems the corresponding ε values are currently unexplored. We will thus consider this case utilizing the PEG-BSA value $\varepsilon = 0.01$[55] stressing that the results shown in the plots have only illustrative value. In addition we will discuss primary adsorption at the wall and brushes containing protein binding ligands tethered at constant altitude z_L, as utilized in PNIPAM based protein chromatography (Figure 1). For simplicity we consider the adsorption modes individually though they may be operative simultaneously.

In every case, we focus on dilute bulk solutions of a single species such that the chemical potential of the free particle is $\mu_{\text{prt}} = k_B T \ln c_{\text{prt}}^b$ where c_{prt}^b is the activity of the particle.[56,57] For the dilute bulk solutions considered the dimensionless c_{prt}^b assumes the value of the molar concentration. In addition the discussion is limited to dilute surface layers such that the interactions between
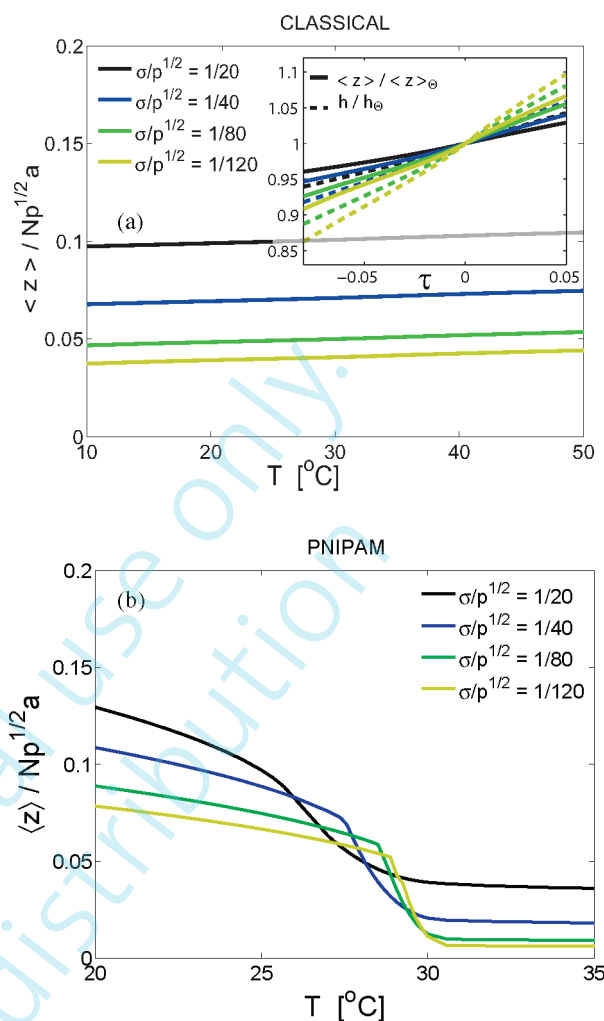
the adsorbed particles can be neglected and their chemical potential is of the form $\mu_{\text{ad}}(z) = k_B T \ln c_{\text{prt}}(z) + F_{\text{att}}(z) + F_{\text{ins}}(z)$. Here $c_{\text{prt}}(z)$ is the particles activity at z within the brush and $F_{\text{att}}(z)$ accounts for the mode specific adsorption free energy. The adsorption isotherms are determined by the equilibrium condition $\mu_{\text{prt}} = \mu_{\text{ad}}(z)$. Among the cases considered it is helpful to distinguish two groups. For weak nonspecific ternary adsorption the particles can adsorb throughout the brush and F_{att} depends on $\phi(z)$ and the surface area of the particle, S_{prt}. In contrast, for primary and ligand adsorption F_{att} is independent of the particle geometry and of $\phi(z)$. In these last two cases the adsorption takes place at a fixed altitude, $z = 0$ and $z = z_L > 0$ respectively. The phenomenological interaction free energies in F_{att}, for example ε, are in general T dependent. However, the T dependence is weak so long as the T interval involved is narrow, as is the case for PNIPAM applications. Accordingly, the T dependence of the adsorption isotherms is dominated
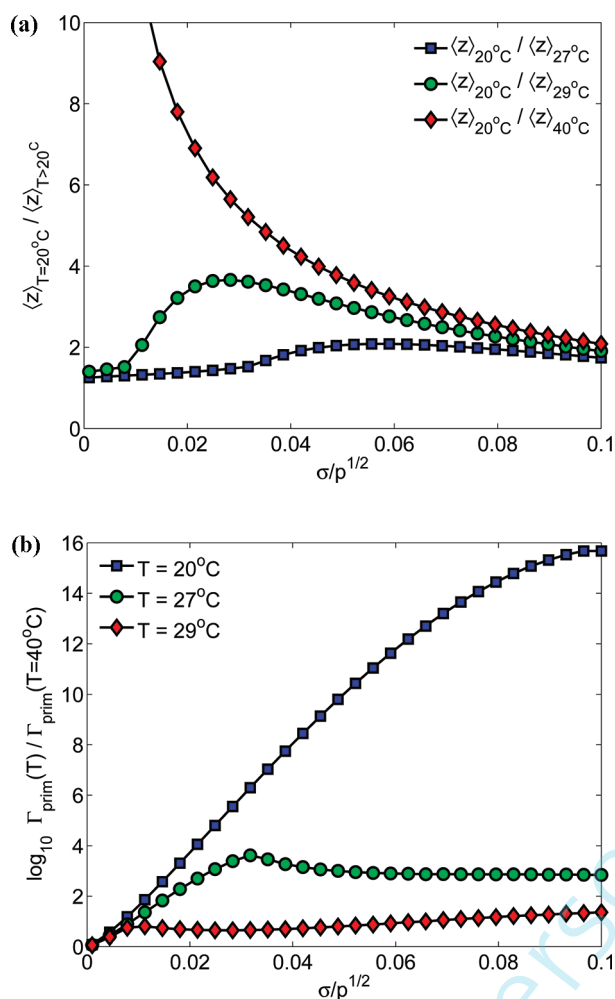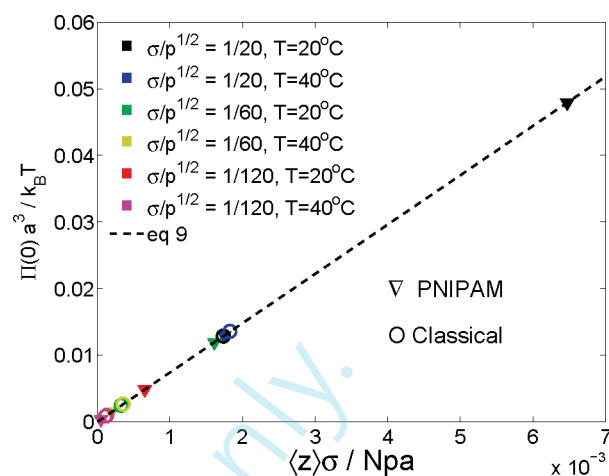
Figure 8. $\Pi(0)a^3/k_BT$ vs $\sigma\langle z\rangle/Npa$ plot collapsing all PNIPAM and classical brush results onto a single curve predicted by eq 9. The results are independent of the choice of a, p, and N.

Figure 7. (a) Plots of $\langle z\rangle_{T=20\,°C}/\langle z\rangle_T$ vs $\sigma/p^{1/2}$ of PNIPAM brush are independent of N. The monotonic curves at $T = 27\,°C$ and $T = 40\,°C$ exhibit opposite slopes while the $T = 27\,°C$ curve displays a maximum. As suggested by eq 17 these features lead to corresponding effects on (b) $\Gamma_{prim}(T)/\Gamma_{prim}^p$. In the plot, $\Gamma_{prim}^p = \Gamma_{prim}(T = 40\,°C)$.

by the contribution of F_{ins}, as given by eq 1, or

$$F_{ins}(z) = \Pi(0)\int_0^h \zeta(z')A_{prt}(z,z')\,dz'$$

$$\equiv \Pi(0)\langle V_{prt}\rangle_\zeta < \Pi(0)V_{prt}(h) < \Pi(0)V_{prt}^0 \quad (14)$$

Here $\zeta(z) = \Pi(z)/\Pi(0)$, $\Pi(0)$ is specified by eq 9 and $\zeta(z) \leq 1$ varies with the model, solvent and T. $V_{prt}(h) \leq V_{prt}^0$ is the geometry and h dependent maximal inserted volume when the particle is in contact with the surface, corresponding to altitude $\hat{z}$:

$$V_{prt}(h) \equiv \int_0^h A_{prt}(\hat{z},z')\,dz' > \langle V_{prt}\rangle_\zeta \quad (15)$$

Here, V_{prt}^0 is the total volume of the particle, and $\langle V_{prt}\rangle_\zeta$ is a $\zeta(z)$ weighted and thus shape dependent effective volume (Figure 1). $\langle V_{prt}\rangle_\zeta$ is well approximated by $\zeta(z)V_{prt}^0$ for fully inserted particles whose vertical span is smaller than h. The T

and Σ dependence is due mostly to $\Pi(0)$ with a weaker contribution arising from $\langle V_{prt}\rangle_\zeta$. Since the SCF $\Pi(z)$ is monotonically decreasing and $\zeta(z) \leq 1$, $\Pi(0)V_{prt}^0$ sets an upper bound for F_{ins}. The leading trends of primary and ligand adsorption of fully inserted particles are recovered, up to numerical factors, by an "Alexander-like" approximation utilizing this upper bound

$$F_{ins} \approx \Pi(0)V_{prt}^0 \quad (16)$$

Within it, the particle experiences a step like $\Pi(z) = \Pi(0)$ extending to $z = h = 2\langle z\rangle$. Note that while eq 16 is reminiscent of eq 5, it differs in that the SCF $\Pi(0)$ is higher than the Π of the Alexander model. The efficacy of this rough approximation depends on the size and altitude of the particle. It improves when two requirements are satisfied. First, the span of the particle along the z axis should be much smaller than h. In this case the particle experiences a slowly varying $\phi(z)$ and $\Pi(z)$. Second, the particle should be situated at the vicinity of the grafting surface $z \gtrsim 0$. This is anyhow the case for primary adsorption. For ligand adsorption the second condition implies short tethers such that the ligand is situated near the surface, $z_L \ll h$. When both conditions are satisfied the particle encounters, in effect, $\phi(0)$ and $\Pi(0)$.

Primary Adsorption. Primary adsorption at the grafting surface is attributed to short ranged attraction between the wall and the particle. Particles at grazing contact with the surface gain an adsorption free energy of $F_{att} = U_{att}$. The values of U_{att} and its T dependence are currently unknown. However, when the T interval considered is narrow one may argue that the T dependence is weak and $U_{att} = $ const. Within the Alexander-like model the free energy of a fully embedded adsorbed particle is thus $F_{prim} = U_{att} + F_{ins} \approx U_{att} + \Pi(0)V_{prt}^0$. Since adsorption is defined by grazing contact it is helpful to define surface concentration $n = \theta n_{sat}$ where n_{sat} is the saturation value in moles per unit area. Accordingly, $\mu_{ad} = F_{prim} + k_BT\ln\theta$ for dilute adsorbed layers with $\theta \ll 1$ and the adsorbed amount per unit area is $\Gamma = c_{prt}^bK_{prim} = c_{prt}^bn_{sat}\exp(-F_{prim}/k_BT)$. We first consider the case of extended brushes such that an adsorbed particle at grazing contact with the surface is fully embedded in the brush irrespective of the solvent quality. Denoting the good and poor solvent values of
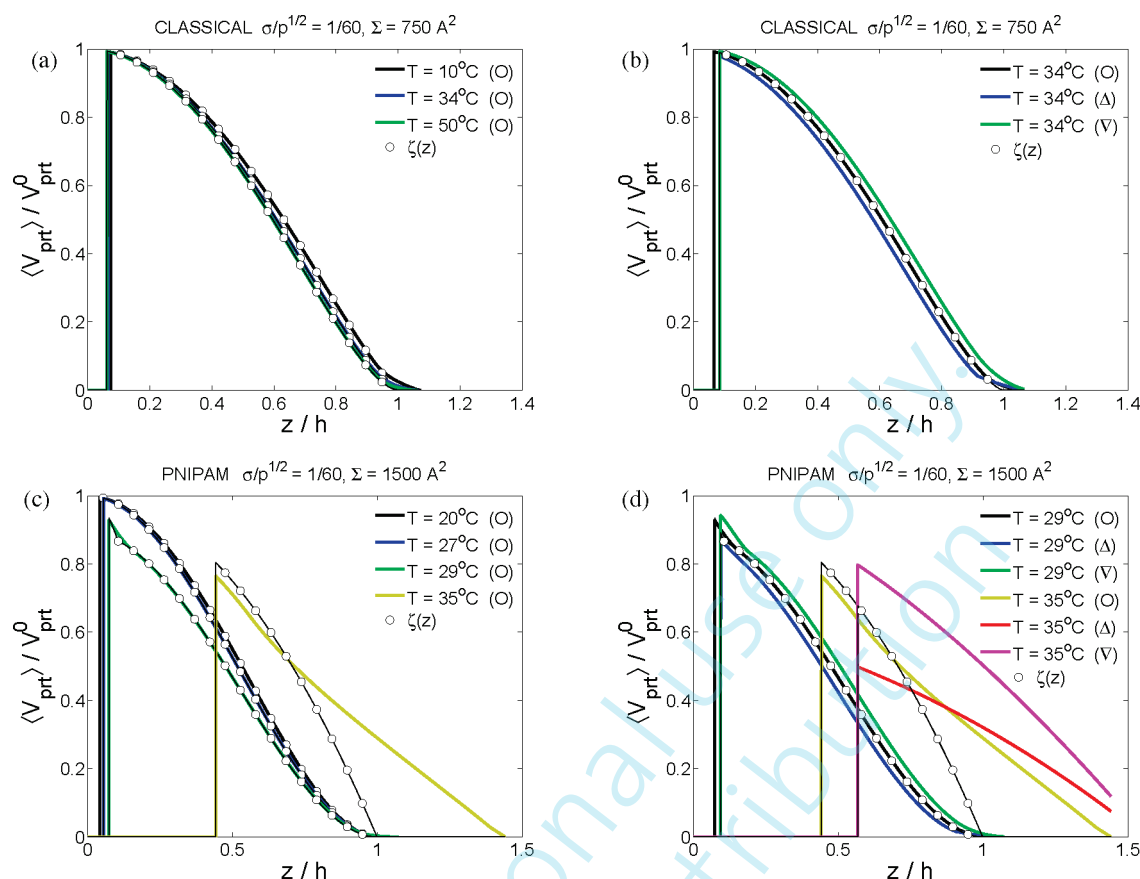
Figure 9. Plots of $\langle V_{prt}\rangle/V_{prt}^0$ vs z/h for different T and particles shapes all having a volume identical to BSA: (a,c) spheres (O) of radius $R = 27$ Å $\ll h$, and (b,d) triangular wedges with their apexes facing the wall (∇) and the bulk (Δ) as obtained for (a, b) classical and (c, d) PNIPAM brushes. Since the plot concerns inserted particles the results are sensitive to the choice of a, p and N. For classical brushes $a = 5/2^{1/4} \approx 4.2$ Å, $p = 2$, $N = 500$ yield semi-quantitatively match to the $\phi(z)$ results reported for polystyrene in cyclohexane, $\Theta = 34$ °C, at $\Sigma = 1660$ Å$^{2.33}$ For PNIPAM $a = 5$ Å, $p = 1$, $N = 500$. $\langle V_{prt}\rangle/V_{prt}^0$ is well approximated by $\zeta(z) = \Pi(z)/\Pi(0)$ (-o-o-o-) when the particle is fully inserted and its span much smaller than h. This is the case for classical brushes in the range 10 °C $\leq T \leq$ 50 °C. Strong deviations due to partial insertion occur for the collapsed PNIPAM brush in part (d).

K_{prim} and Γ_{prim} by the superscripts g and p eqs 4 and 11 lead to

$$\frac{\Gamma_{prim}^g}{\Gamma_{prim}^p} = \frac{K_{prim}^g}{K_{prim}^p} = \exp\left[-\frac{\Pi_g(0)V_{prt}^0 - \Pi_p(0)V_{prt}^0}{k_B T}\right]$$

$$= \exp\left[-\frac{\Pi_g(0)V_{prt}^0}{k_B T}\left(1 - \frac{\langle z\rangle_p}{\langle z\rangle_g}\right)\right] < 1 \text{ (full insertion)}$$

(17)

$\Gamma_{prim}^g/\Gamma_{prim}^p < 1$ because of $\langle z\rangle_p/\langle z\rangle_g < 1$ manifesting the higher osmotic penalty incurred in good solvent. The T dependence of $\Gamma_{prim}^g/\Gamma_{prim}^p$, as given by eq 17 upon substitution of the T dependent $\langle z\rangle_p/\langle z\rangle_g$ recovers the exact SCF results as obtained from $\Gamma_{prim}^g/\Gamma_{prim}^p = \exp[-F_{ins}(g)/F_{ins}(p)]$. However, the T dependence of $\langle z\rangle_p/\langle z\rangle_g$ assumes different forms for PNIPAM and for classical brushes (Figures 6 and 7). Thus, $\Gamma_{prim}(T)/\Gamma_{prim}(40\ °C)$ of classical brushes decreases with increasing T while PNIPAM brushes exhibit the opposite behavior (Figure 10).

For fully inserted particles, the effect is independent of N. However, a particle at grazing contact with the surface protrudes out of the brush when its size along the z axis is large in comparison with h. Only the inserted volume of the particle,

$V_{prt}(h) < V_{prt}^0$ affects $\Gamma_{prim}^g/\Gamma_{prim}^p$ and $V_{prt}(h)$ depends on the geometry of the particle. To capture the qualitative features of this effect we utilize, for simplicity, the Alexander-like approximation stressing that quantitative results require numerical solution of the SCF equations. In particular we consider a cylindrical particle of height $L_{cyl} > h$ inserted with its base grazing the surface. The inserted cylindrical volume in this approximation is $V_{cyl}(h) = V_{cyl}^0 h/L_{cyl}$ and $\Pi_i(0)V_{cyl}^0$ is replaced by $\Pi_i(0)V_{cyl}(h)$. $\Gamma_{prim}^g/\Gamma_{prim}^p$ for the case $L_{cyl} > \langle z\rangle_g > \langle z\rangle_p$ is thus

$$\frac{\Gamma_{prim}^g}{\Gamma_{prim}^p} = \frac{K_{prim}^g}{K_{prim}^p}$$

$$= \exp\left[-\frac{\Pi_g V_{cyl}(h_g)}{k_B T}\left(1 - \frac{\langle z\rangle_p^2}{\langle z\rangle_g^2}\right)\right] \text{ (partial insertion)}$$

(18)

and the reduction in $\Gamma_{prim}^g/\Gamma_{prim}^p$ is N dependent because $V_{cyl}(h_g) \sim h_g \sim N$.

In comparison to the Alexander like approximation, the full SCF results are modified because $\Pi_i(0)V_{prt}^0$ is replaced by $\Pi_i(0)\langle V_{prt}\rangle_\zeta$ which depends on $\zeta(z)$ as well as on the geometry

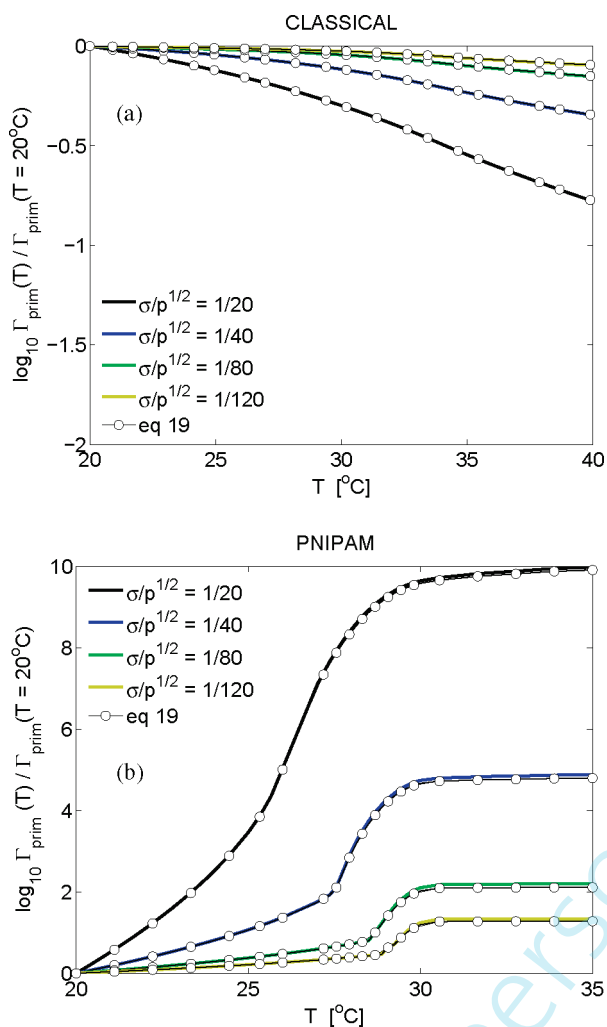**Figure 10.** $\log_{10}\Gamma_{\text{prim}}(T)/\Gamma_{\text{prim}}(T = 20\,°C)$ vs T for primary adsorption of spherical particles having the volume of BSA onto surfaces displaying (a) classical and (b) PNIPAM brushes at several $\sigma/p^{1/2}$. In both cases the results are well approximated by eq 17 however plots of PNIPAM and classical brushes exhibit opposing T dependence, different range and distinctive shapes traceable to the T dependence of $\Pi(z)$ and $\langle z \rangle$. Brush parameters as for Figure 9.

of the inserted particle. This effect certainly affects the partial insertion case and eq 18. However, for primary adsorption of relatively small particles there are no qualitative differences between the Alexander-like approximation and the SCF description because the particles are localized at the vicinity of the grafting surface, $z \gtrsim 0$, and the precise form of $\phi(z)$ does not play a crucial role (Figure 10). Utilization of the rigorous SCF results in this case is not necessarily useful in view of the approximations anyhow involved: overlooking the depletion layer at the wall, the role of surface roughness and the exact form of the particle. Note finally that our discussion focused on a single component bulk solution. For dilute multicomponent solution $\Gamma = \sum c_p(i)K_{\text{prim}}(i)$ where i labels the species involved.

Tethered Ligand at z_L. In the primary adsorption scenario the particles adsorb at $z = 0$ and the details of the concentration profile have relatively minor effect. This situation is modified when the particles bind to a ligand at a fixed altitude $z_L > 0$ within

the brush, a picture suggested for the chromatographic matrices developed by Yoshizako et al.[5] We consider dilute ligands with a surface concentration n_L low enough to ensure no interaction between the complexed ligands, even at saturation. In this case, the particle-ligand binding free energy, F_L, is essentially constant for the narrow T range encountered in PNIPAM applications. The equilibrium fraction of ligands binding particles, X, is specified by $X/(1 - X) = c^b_{\text{prt}}K^i_L$ where the binding constants within the brush $K^i_L = \exp[-(F_L + F_{\text{ins}})/k_BT]$, $i = g,p$, assume different forms in good and poor solvents because of F_{ins}. For simplicity we focus on the linear regime $X = c^b_{\text{prt}}K^i_L$ obtained when $X \ll 1$. It is helpful to consider three cases: (i) when $z_L > h_g > h_p$ the brush has no effect, $K^g_L/K^p_L = 1$, since $F_{\text{ins}} = 0$ for both good and poor solvents; (ii) if $h_g \gg z_L > h_p$ only K^g_L is lowered because of the brush insertion penalty and thus $K^g_L/K^p_L < 1$; (iii) when $h_g > h_p \gg z_L$ both K^g_L and K^p_L are reduced and $K^g_L/K^p_L < 1$ because F_{ins} in poor solvents is lower. The qualitative features are evident within the Alexander-like approximation. Focusing on the full insertion scenario for $h_g > h_p \gg z_L$

$$\frac{\Gamma^g_L}{\Gamma^p_L} = \frac{K^g_L}{K^p_L}$$

$$= \exp\left[-\frac{\Pi_g(0)V^0_{prt}}{k_BT}\left(1 - \frac{\langle z \rangle_p}{\langle z \rangle_g}\right)\right] > \exp\left[-\frac{\Pi_g(0)V^0_{prt}}{k_BT}\right] \tag{19}$$

where the RHS specifies $\Gamma^g_L/\Gamma^p_L = K^g_L/K^p_L$ for $h_g \gg z_L > h_p$. Note that within this approximation this K^g_L/K^p_L is indistinguishable from $K^g_{\text{prim}}/K^p_{\text{prim}}$ given by eq 17 (Figure 10). While the Alexander-like approximation captures the qualitative effect it is misleading in that it suggests that the choice of z_L has no effect once the range $h_g > z_L > h_p$ or $h_g > h_p > z_L$ was set. The SCF version, reflecting the full eq 14,

$$\frac{K^g_L}{K^p_L} = \exp\left[-\frac{\Pi_g(0)\langle V_{\text{prt}}\rangle_\varsigma(g)}{k_BT} + \frac{\Pi_p(0)\langle V_{prt}\rangle_\varsigma(p)}{k_BT}\right] \tag{20}$$

reveals an additional z dependence due to $\langle V_{\text{prt}}\rangle_\varsigma$ and reflecting the shape specific $A_{\text{prt}}(z)$ and the solvent and model specific $\Pi(z) = \Pi(0)\zeta(z)$ (Figure 11). To gain insight concerning this aspect it is helpful to consider semidilute classical brushes (Appendix A). A simple analytical expression for K^g_L/K^p_L can be obtained for small spherical particles with radius $R_{\text{prt}} \ll h$. In this case $F_{\text{ins}} \approx \Pi(z_L)V^0_{\text{prt}}$ because $\phi(z)$ changes slowly over a distance R_p and the errors incurred at the inner and outer edges of the particle tend to cancel. For classical brushes in the $|\tau| \gg 1$ range $\Pi_g(z)a^3/k_BT = (9\pi^{4/3}/16)\tau^{1/3}\sigma^{4/3}p^{-2/3}(1 - z^2/H^2_g)^2$ and $\Pi_p(z)a^3/k_BT = (3\pi^2/4)w|\tau|^{-1}\sigma^2p^{-1}(1 - z^2/H^2_p)$.[34] Accordingly

$$\frac{K^g_L}{K^p_L} = \exp\left\{-\frac{\Pi_g(0)V^0_{\text{prt}}}{k_BT}\left[\left(1 - \frac{z^2_L}{h^2_g}\right)^2 - \frac{4}{3}\frac{h_p}{h_g}\left(1 - \frac{z^2_L}{h^2_p}\right)\right]\right\}$$

$$> \exp\left[-\frac{\Pi_g(0)V^0_{\text{prt}}}{k_BT}\left(1 - \frac{z^2_L}{h^2_g}\right)\right] \tag{21}$$

where the RHS corresponds again to K^g_L/K^p_L for $h_g > h_p \geq z_L$ as considered within the Alexander like approximation. However, in distinction, the highest possible K^g_L/K^p_L is now
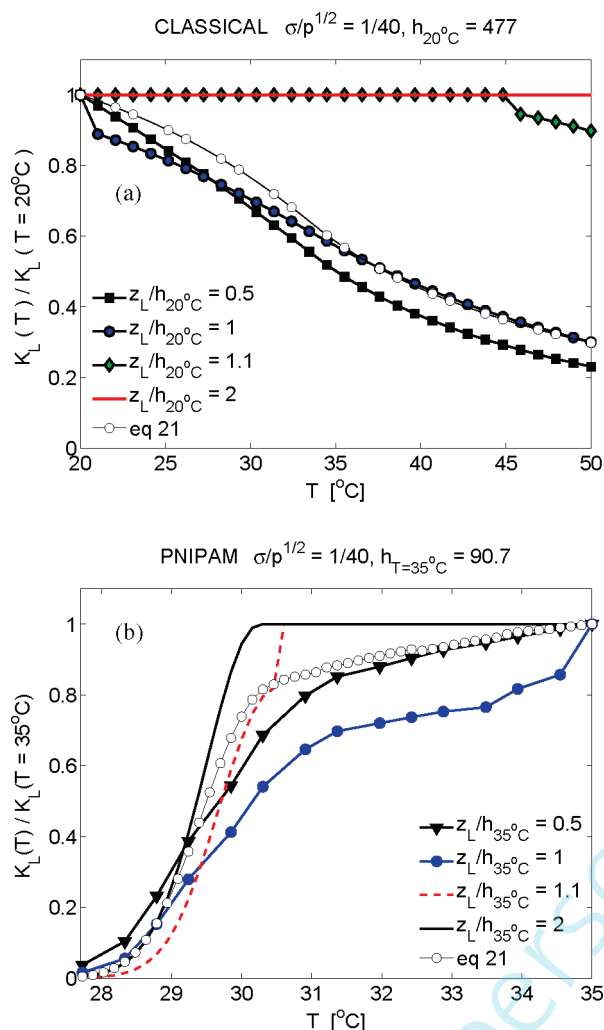
Figure 11. $\Gamma_L^g/\Gamma_L^p = K_L^g/K_L^p$ vs T for ligand adsorption at different ligand altitudes z_L/h for (a) classical and (b) PNIPAM brushes. The poor solvent reference for classical and PNIPAM brush are respectively $T = 20$ °C and $T = 35$ °C. Equation 19 largely captures the behavior of Γ_L^g/Γ_L^p of deeply inserted ligands. The behavior for high z_L is less sensitive to the brush. Brush parameters as for Figure 9.

obtained at a specific z_L namely $z_L = h_p$ where

$$\frac{K_L^g}{K_L^p} = \exp\left[-\frac{\Pi_g(0)V_p^0}{k_B T}\left(1 - \frac{h_p^2}{h_g^2}\right)\right] \quad (22)$$

The σ dependence of the exponent in eq 22 is due to $\Pi_g(0)$ and to $1 - h_p^2/h_g^2$. It thus varies as $\sigma^{4/3}(1 - D\sigma^{4/3})$ with $D = \pi^{4/3}/4(\phi_p^3 p\tau)^{2/3}$ thus suggesting an optimal grafting density $\sigma_{\rm opt} = (1/2D)^{3/4} \approx 0.5(\phi_p^3 p\tau)^{1/2}$ subject to the requirement that N is large enough so that the brush regime is attained irrespective of the solvent quality. This requirement favors large N thus leading to large h_p and large $z_L > h_p$. The design of long rigid spacers setting a fixed z_L is not evident and the use of flexible spacer requires a somewhat modified analysis allowing for the stretching of the tether chain upon complexation of the ligand with the particle. Note that our numerical results regarding binding within a classical brush concern the near Θ regime where $\Pi(z) \sim \phi^3(z)$ rather than $\Pi(z) \sim \phi^2(z)$

and thus[34]

$$\frac{K_L(T)}{K_L(\Theta)} = \exp\left\{-\frac{\Pi_\Theta(0)V_{prt}^0}{k_B T}\left[\frac{H^3}{H_\Theta^3}u^{3/2}\left(\frac{z_L}{H}\right) - u^{3/2}\left(\frac{z_L}{H_\Theta}\right)\right]\right\} \quad (23)$$

In any case, the above expressions are applicable in a limited T range. As a result the $\Pi(z)$ curves deviates weakly from the analytical SCF results in the T range explored numerically (Figures 3 and 4). In turn these small deviations are exponentially amplified in K_L thus requiring full implementation of the numerical SCF solutions (Figure 11).

A. Comment on Weak Ternary Adsorption in Non-Classical Brushes Undergoing Vertical Phase Separation. As noted earlier, the adsorption behavior depends on the characteristics of the free energy driving it, $F_{\rm att}$. Here we focus on the case of pure ternary adsorption arising because of weak nonspecific monomer-particle attraction.[21,23,46] In this scenario the surface of the particle is assumed to be uniform and a monomer at grazing contact with the particle is assigned an energy of $-\varepsilon k_B T$ with $0 < \varepsilon \ll 1$ to ensure that there is no distortion of the brush concentration profile. This last requirement is necessary to justify the assumption of the insertive mode and the applicability of eq 1. Altogether, $c_{\rm prt}(z)$ reflects the interplay of $F_{\rm ins}(z)$, as given by eq 1, and

$$\frac{F_{\rm att}(z)}{k_B T} = -\frac{\varepsilon}{a^2}\int_0^h \phi(z')S_{\rm prt}(z,z')\,dz' \quad (24)$$

where $S_{\rm prt}(z,z')\,dz'$ is the surface area increment over the interval $[z', z' + dz']$ of a particle whose center of mass is at z. A systematic study of weak ternary adsorption in classical brushes was reported earlier.[23,34] Here we comment on the distinguishing features of the case of nonclassical PNIPAM brushes exhibiting a vertical phase separation. The numerical results (Figure 12b) for PNIPAM are obtained using $f_{\rm int}$ Afroze et al.[15] and assuming $\varepsilon = 0.01$ suggested for BSA–PEG interactions.[55] In contrast to classical brushes (Figure 12a), in this case $c_{\rm tern}(z)$ is no longer monotonic. Rather, it develops a maximum at the vicinity of the phase boundary. $F_{\rm att} \sim \phi$ favors insertion at the inner and denser side of the discontinuity in $\phi(z)$ since $F_{\rm att}$ is much weaker at the outer side. This tendency is not smeared out by $F_{\rm ins}$ because $\Pi(z)$, in contrast to $\phi(z)$, is continuous at the boundary. Similar effects are expected in the strong adsorption scenarios. Note, however that our exploratory analysis assumes that a single $0 < \varepsilon \ll 1$ characterizes all monomers. This assumption is supported by experimental data for the case of PEG[55] but remains to be studied for PNIPAM. Furthermore, this description may require revision in order to allow for two-state models of the polymer (Appendix A), protein surface domains[23] etc. For example, a minimal description invoking a two-state model requires the introduction of two different ε.

V. DISCUSSION

Adsorption onto surfaces displaying polymer brushes is opposed by an insertion penalty, $F_{\rm ins} = \Pi(0)\langle V_{\rm prt}\rangle_\xi$. $F_{\rm ins}$ reflects the effects of particle insertion on the interaction and elastic free energies of the chains. It assumes the form of work done in overcoming the osmotic pressure of the unperturbed brush upon insertion of the impenetrable particle. Brush collapse is associated with lower $\langle z \rangle$ and thus favors adsorption because of the
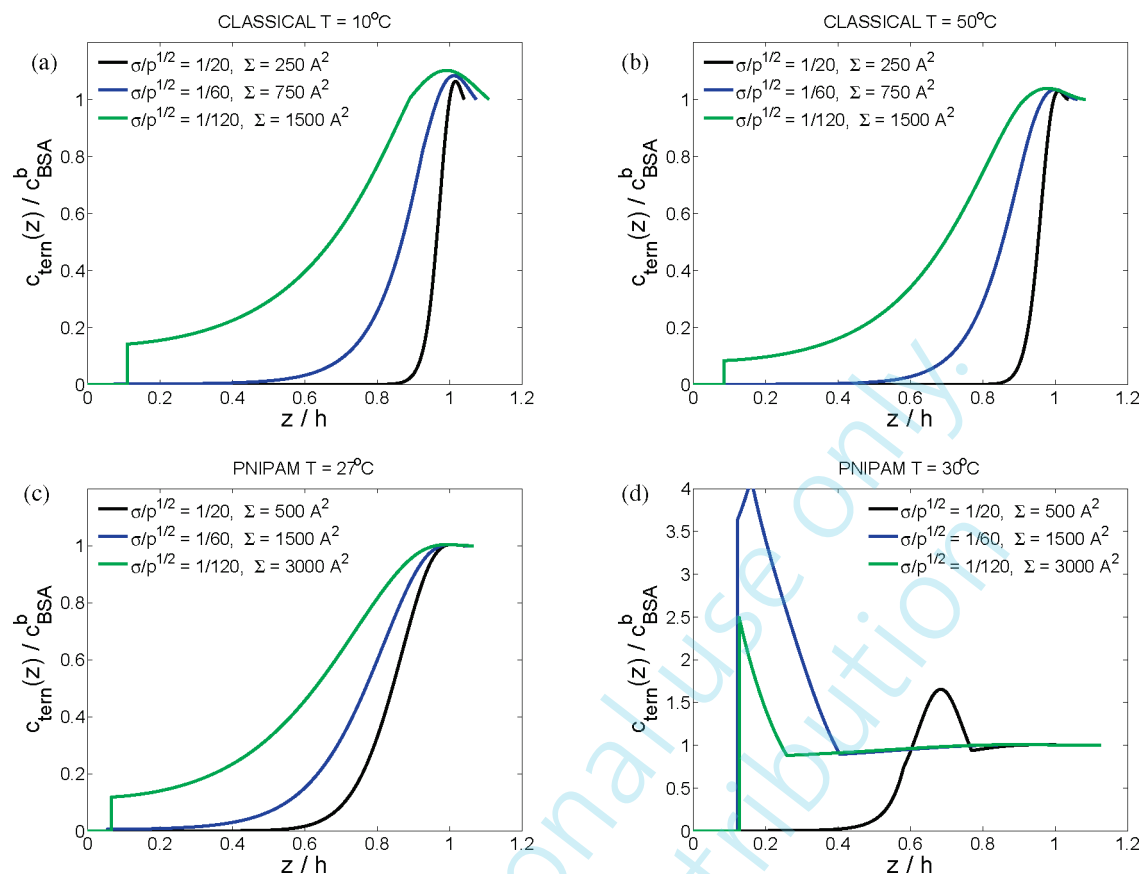
Figure 12. $c_{prt}(z)/c_{prt}^b$ vs z/h for weak ternary adsorption of spherical particles of radius $R = 27$ Å, corresponding to BSA volume, onto (a,b) classical and (c,d) PNIPAM brushes at different T and $\sigma/p^{1/2} = a^2/\Sigma p^{1/2}$. In both cases $\varepsilon = 0.01$ and the brush parameters are as in Figure 1. The mostly monotonically increasing $c_{prt}(z)$ in parts a—c are associated with continuous $\phi(z)$ while the pronounced maxima in part d are traceable to a vertical phase separation leading to discontinuous $\phi(z)$. The weak maxima in parts a—c at $z \approx h$ are traceable to partial insertion and increase further with increasing R (results not shown). Bulk concentration $c_{prt} = c_{BSA}^b$ is attained at grazing contact with the brush, at $z = h + R$.

lower F_{ins}. The reduction in F_{ins} is due to two effects: First, $\Pi(0)a^3/k_B T \approx \sigma\langle z\rangle/Npa$ (eq 9) decreases with $\langle z\rangle$. Second, the inserted volume of the particle may also decrease upon collapse thus lowering $\langle V_{prt}\rangle_\xi$. Adsorption is favored by collapse in spite of the higher brush density because poorer solvent quality lowers $\Pi(z)$ and h at a given Σ. The opposite trend occurs when the brush density increases upon increasing the grafting density at constant T. This picture is independent of the nature of the polymers forming the brush, the solvent or the adsorbing colloids. It applies when the insertion scenario is realized, i.e., when a particle placed inside the brush can be circumvented by the chains trajectories and when the polymer—particle interactions induces only short ranged perturbation of the concentration profile. With these caveats it pertains to protein adsorption onto PNIPAM bearing brushes in water as well as to colloid adsorption in non-aqueous solvents.

The variation of F_{ins} with $\langle z\rangle$ rationalizes qualitative trends concerning the effect of collapse on adsorption onto brushes. To obtain quantitative results it is necessary to consider a specific adsorption mechanism and the corresponding balance of $F_{ins} = \Pi(0)\langle V_{prt}\rangle_\xi$, opposing adsorption, and an attractive free energy driving it, F_{att}. In applying this analysis it is helpful to distinguish between two situations differing in their reliance on an explicit f_{int}. For certain adsorption mechanisms, it is possible to relate the results of two families of experiments with no prior assumptions

concerning f_{int}. Such "arbitrary f_{int}" analysis allows to predict the T dependence of the adsorption isotherms of a given brush in terms of the measured $\langle z(T)\rangle$ of its unperturbed counterpart. The biotechnology applications of PNIPAM brushes harness the general features of the collapse effect as summarized earlier and can be analyzed via the arbitrary f_{int} approach. However, the collapse of PNIPAM is uniquely compatible with biotechnology applications because it occurs in water and at narrow T interval near ambient T, conditions that are not damaging to cells and to proteins. Importantly, the T dependence of $\langle z\rangle$, $\phi(z)$ and the adsorption isotherms require explicit f_{int}, a and p and can not be predicted using the arbitrary f_{int} results.

The "arbitrary f_{int}" analysis yields useful results when the adsorption takes place at fixed z and both F_{ins} and F_{att} are independent of the detailed $\phi(z)$. Such is the case for primary adsorption at the wall, $z = 0$, and ligand adsorption at $z = z_L \ll \langle z\rangle$. In these two situations the effect of collapse on the adsorption isotherms of fully inserted particles is approximated by eq 17. For the case of protein adsorption onto PNIPAM brushes eq 17 suggests two experiments each utilizing brushes with constant σ and N: (i) The first is measuring the ratio Γ^g/Γ^p for a given protein and brush utilizing a fixed good solvent T, T_g, while varying the poor solvent T, T_p. In this case the ratio ratio $\Gamma^g(T_g)/\Gamma^p(T_p)$ will vary with T_p via the experimentally measurable $\langle z(T_p)\rangle/\langle z(T_g)\rangle$ (Figure 10). (ii) In the second option V_{prt}^0 is

varied by utilizing different proteins with identical binding properties. This option is especially attractive for ligand binding with BSA[5] because it is possible to produce Cibacron Blue binding BSA fragments by chemical cleavage or by molecular cloning.[53] The ratio of the two Γ^g/Γ^p is then predicted to follow

$$\frac{\Gamma^g_{BSA}/\Gamma^p_{BSA}}{\Gamma^g_{frag}/\Gamma^p_{frag}} = \exp\left[-\frac{\Pi_g(0)V^0_{BSA}}{k_B T}\left(1 - \frac{V^0_{frag}}{V^0_{BSA}}\right)\left(1 - \frac{\langle z\rangle_p}{\langle z\rangle_g}\right)\right] > \frac{\Gamma^g_{BSA}}{\Gamma^p_{BSA}}$$

(25)

where V^0_{frag}/V^0_{BSA} for reported fragments is roughly 1/3.

The RHS of eq 17 may be specified in terms of experimental data on V^0_{prt}, $\langle z\rangle$ and σ with no explicit knowledge of $\phi(z)$ and $\Pi(z)$. When applicable, it is of interest because of the current uncertainties concerning the PNIPAM f_{int}, a and p. However, detailed analysis requires knowledge of f_{int} thus enabling the calculation of the T dependent $\phi(z)$ and $\Pi(z)$ in order to obtain $\Pi(0)$ and $\langle V_{prt}\rangle_\zeta$. The case of nonaqueous solvents, when the brush behavior is classical and $f_{int}a^3 = \hat{v}\phi^3 + \hat{w}\phi^3$, was recently analyzed.[34] The situation is more difficult when considering NWSP in water. The classical description applies to PEG brushes at near ambient T, far below its LCST (Appendix A). It is not applicable to PNIPAM brushes whose biotechnology applications take place at the vicinity of the LCST. The current experimental evidence concerning PNIPAM brushes suggests nonclassical behavior involving vertical phase separation. Since a molecular model consistent with the experiments is yet to emerge we based our analysis on an empirical f_{int} proposed by Afroze et al. because it suggests a phase diagram consistent with the reported vertical phase separation. The implementation of the SCF theory utilizing this model requires numerical solution because higher order virial terms are important. It yields SCF $\phi(z)$ and $\Pi(z)$ profiles and their dependence on Σ and T. The PNIPAM results differ qualitatively from the corresponding "classical" plots. The differences concern the T dependence of $\langle z\rangle$ and $\Pi(z)$ as well as the discontinuity in $\phi(z)$ and discontinuities in the slopes of $\Pi(z)$. The classical brush $\langle z\rangle$ and $\Pi(0)$ weakly increase with increasing T while their PNIPAM counterparts strongly decrease. Nevertheless, all results, irrespective of the model, are consistent with eq 9 (Figure 8). The variation of $F_{ins} = \Pi(0)\langle V_{prt}\rangle_\zeta$ with T semi-quantitatively accounts for the observed trends concerning protein adsorption and cell adhesion.

In envisaging detailed comparison with experiments and simulations it is important to note the limitations of the theory as well as experimental lacunae. The analytical SCF theory we utilize does not describe depletion at the wall nor does it allow for fluctuation effects. In particular, it translates bulk binodals into sharp boundaries rather than into diffuse interfaces. The theory focuses on uniform and monodispersed brushes grafted onto planar surfaces. It does not allow for polydispersity in N and Σ or for surface roughness. Within the SCF theory p is a constant exhibiting no T dependence. This picture can not allow for cooperative hydration of PNIPAM, as suggested by experiments[58] and theory.[59] Our discussion of PNIPAM brushes utilized the empirical f_{int} obtained by Afroze et al. by fitting experimental points on the PNIPAM—water phase boundary. As noted by Afroze et al., this f_{int} does not allow for polydispersity, it applies a limited T range and it does not reproduce well all of the experimental points. Furthermore, the differences between the results of Afroze et al.[15] and of Rebelo et al.[43] remain to be clarified (Appendix A). Additional difficulties arise because of the

current uncertainties regrading a and p of PNIPAM (Appendix A). These are amplified by experimental difficulties in characterizing N and Σ, especially when the brushes are produced by grafting from methods. Finally, our analysis considers equilibrated systems and overlooks kinetic effects playing a role for short incubation times.

The points listed above concern issues related to brush structure in the absence of adsorbing particles. Additional experimental issues arise when considering the interactions of PNIPAM brushes with proteins and cells. These are similar to difficulties in characterization of the interactions between proteins and PEG brushes. One issue concerns the protein concentration profile within the brush, $c_{prt}(z)$. This is important in order to distinguish between primary adsorption at the wall, ternary adsorption within the brush and secondary adsorption at its outer edge. However, most experimental techniques measure Γ but can not characterize the protein $c_{prt}(z)$ and the adsorption modes. The current evidence for different protein adsorption modes is indirect and based on the Σ dependence of Γ. Neutron reflectometry utilizing deuterated proteins may enable to resolve this question for certain proteins.[60] A related problem concerns the interactions between NWSP and proteins. Ternary adsorption is only possible for proteins having attractive interactions to NWSP. Some evidence for attractive interactions between proteins and NWSP, both PEG and PNIPAM, was already reported.[55,61,62] However, these interactions were studied only for limited number of proteins and with rare exceptions[63] the results do not shed light on their specificity. In contrast to the interactions between serum albumin with small ligands,[54] little is known about polymer binding sites and their distribution on the surface of the protein. We should add that the formulation of a SCF theory of swollen brushes explicitly incorporating colloidal particles is yet to be attained. While such theory was formulated for dry brushes[64] its generalization to the case of particles inserted into swollen brushes is non trivial.

Finally, it is helpful to comment on the role of computer simulations in this area. Computer simulations confronting SCF results for semidilute classical brushes do not require an explicit solvent. When solvent particles are introduced, spherical particles with isotropic interactions suffice to describe classical brushes. "Solvent free" simulations allowed to investigate F_{ins}[22,25] while explicit solvent simulations were used to probe the concentration profile of adsorbing colloidal particles.[65] In both cases the studies involved good solvent conditions and insertion into collapsed classical brushes remains to be studied. In contrast, the simulation of PNIPAM brushes in aqueous media requires explicit solvent because directional H-bonds with water play an essential role. So far only simulations involving single PNIPAM chains in water were reported.[66−68] They produce a wealth of information about the chain configurations as well as the number of different H-bonds in water and around the chain. However, it is difficult to extract from the simulations the parameters that were invoked in theoretical models of NWSP in water. In addition, such simulations involve particular choices for the force fields and the definitions of H bonds. In turn, the results are sensitive to these choices.[68] As a result simulation of adsorption onto PNIPAM brushes is currently a challenging problem and confrontation with SCF theory is not an immediate prospect.

With the reservations noted above our theoretical analysis suggests experimental exploration of three accessible effects. First, the investigation of the relationship between $\langle z\rangle$ of the unperturbed, protein free brush and the protein adsorption

isotherms. Second, the utilization of protein fragments to explore size effects on the adsorption behavior. Finally, comparison of the T dependence of the experimentally acquired protein adsorption isotherms to the predictions based on the f_{int} of Afroze et al.[15] Our analysis focused on the tuning of protein adsorption via temperature induced brush collapse/swelling. However, related considerations are also of relevance to the control of cell adhesion when adhesion proteins are involved. In this context it is important to note first that cell size is of order of 10 μm and thus much larger than a typical brush h. As a results cells can only approach the grafting surface by compressing the brush. The associated free energy penalty is high and the proximal cell membrane is thus located at $z \simeq h$. Accordingly, brush collapse can affect cell adhesion because the interactions between the cells and the surface diminish as h increases. This is the case, for example, for van der Waals attraction. h may also affect cell binding to adhesion proteins adsorbed at the grafting surface. The effects noted above are independent of F_{ins} incurred by adhesion proteins inserted into the brush. However, in addition the adsorption of adhesion proteins within the brush is weakend by F_{ins} and thus favored by collapse, as discussed previously.

APPENDIX A: CLASSICAL VS NON-CLASSICAL BRUSHES AND PNIPAM

Our discussion and analysis reflect an extensive literature concerning classical and non classical brushes as well as PNIPAM, its f_{int}, phase behavior, interactions with proteins and molecular parameters. The relevant items are summarized in this Appendix.

1. Classical and Non-Classical Brushes, PNIPAM and Its f_{int}. The SCF theory of brushes typically invokes f_{int} specified by a virial expansion[26,27]

$$f_{int}a^3 = \hat{v}\phi^2 + \hat{w}\phi^3 + ... \tag{A1}$$

where $\hat{v}$ and $\hat{w}$ denote the a and p ($= l_p/a$) independent *dimensionless* second and third virial coefficients. These may be determined empirically or from the monomer—monomer interaction potential. For classical systems, when the potential comprises of hard core with a fast decaying attraction $\hat{v} \approx \tau \equiv 1 - \Theta/T$ and $\hat{w} \approx$ const. However, each virial coefficient may in principle be negative and capable of changing sign. The empirical description of PNIPAM solutions involves a somewhat different formulation based on a modification of the Flory—Huggins (FH) mixing free energy.[26,27] For a brush of immobile chains the $N \to \infty$ limit is applicable and the FH f_{int} reduces to

$$f_{int}a^3 = (1 - \phi)\ln(1 - \phi) + \chi\phi(1 - \phi) \tag{A2}$$

Here χ is the T dependent Flory interaction parameter and $\chi > 0$ for non—polar monomers interacting via dispersion forces. In the FH theory $\chi = \chi(T)$ is independent of ϕ. Within this picture, corresponding to classical brushes, polymer solutions exhibit only an upper critical solution temperature (UCST). In the limit of $N \to \infty$ the UCST occurs at $\phi = 0$ and $\chi_c = 1/2$. The resulting coexistence curve involves equilibrium between a polymer solution and a pure solvent. Importantly, this f_{int} can not describe a phase diagram exhibiting a LCST. A phenomenological generalization of the FH f_{int} involves the replacement of $\chi(T)$ by an effective $\chi_{eff} = \chi(T,\phi)$,[69] which may be expressed as $\chi_{eff} = \Sigma_i \hat{\chi}_i(T)\phi^i$. Recall that the expansion of the FH f_{int} yields $\hat{v} = (1 - 2\chi)/2$ and this is the only virial coefficient that can change

sign while all higher order coefficients are positive with values set by eq A2. This situation changes for non classical systems when $\chi_{eff} = \chi_{eff}(T,\phi)$ replaces $\chi(T)$ and the values of the virial coefficients are influenced by the $\hat{\chi}_i$ values. In particular, introducing $\chi_{eff} = \chi_{eff}(T,\phi)$ or the equivalent modification in the virial coefficients can change the critical behavior of the solution. First, this allows to describe a high T insolubility loop with both LCST and UCST thus enabling the description of NWSP polymers exhibiting a LCST. Second, it can gives rise to a "second type of phase transition" such that $\phi_c > 0$ at $N \to \infty$ and the phase diagram involves coexistence between two polymer solutions of finite concentrations, $\phi_+(T) > \phi_-(T)$.[70,71] This last effect has a qualitative impact on the brush structure. Since the exchange chemical potential $\mu(\phi(z))$ of a monomer in the brush is parabolic in z, the phase equilibrium condition $\mu(\phi_+) = \mu(\phi_-)$ (Appendix D) can give rise to a vertical phase separation manifesting itself by a discontinuity in $\phi(z)$.[28−31]

The two parameter $f_{int}a^3 = \hat{v}\phi^2 + \hat{w}\phi^3$ description was utilized to discuss classical brushes. The behavior of non-classical brushes of NWSP in water reflects an additional family of monomeric interactions due to formation of H-bonds. The classical brush theory can capture the behavior of water swollen brushes far below the LCST, as is the case for PEG. However, this description is not applicable at the vicinity of the LCST, the relevant regime for the discussion of the collapse of PNIPAM brushes. To describe this last regime it is necessary to introduce $\chi_{eff} = \chi_{eff}(T, \phi)$, either as an empirical relation or from a theoretical model. This brings us to the phase diagram of PNIPAM and the $\chi_{eff}(T,\phi)$ proposed to fit it.

A full consensus regarding the phase behavior of PNIPAM solutions is yet to emerge.[15,40−43] Two recent reports highlight the problem. Rebelo et al.[43] report a LCST at $T_c = 306.4$ K and $\phi_c = 0.13$. Their measurements and analysis suggest that the binodal is essentially horizontal in the range $0 < \phi < 0.8$. In contrast Afroze et al.[15] identified a LCST at $T_c = 299.5$ K and polymer mass fraction of $w_c = 0.43$ with a curved binodal reaching $T \simeq 304$ K in the dilute limit. Their analysis suggests that PNIPAM undergoes a second type of phase transition. The results of both studies were also formulated in the form of $\chi_{eff} = \Sigma\hat{\chi}(T)\phi^i$. Experimental $\phi(z)$ curves for PNIPAM brushes suggests vertical phase separation with coexistence of $\phi_+ \approx 0.6$ with $\phi_- \approx 0.2-0.3$ at $T = 305$ K.[16,17] This picture is inconsistent with the horizontal binodal of Rebelo *et al.*.[43] We thus based our discussion on the empirical $\chi_{eff} = \Sigma_i\hat{\chi}(T)\phi^i$ of Afroze et al.[15] that yields $\phi(z)$ consistent with the experimental results though at slightly different temperatures. This picture is also supported by recent results of Zhou et al.[72] who found $\phi_c^{LCST} \approx 0.4$ and $T_c^{LCST} \approx 301.8$ K. However, it is important to note that the $\phi(z)$ profiles obtained from the Afroze $\chi_{eff} = \chi_{eff}(T,\phi)$ provide a necessary but insufficient ingredient for discussing the physical chemistry of PNIPAM brushes: wetting behavior or the aggregation of colloidal particles bearing PNIPAM brushes. To identify the missing ingredients it is helpful to relate χ_{eff} to theoretical models. We are unaware of a theoretical model corresponding quantitatively to the data of Afroze et al.[15] However there is a large group of models concerning solutions of H-bond forming polymers.[73−80] These were mostly motivated by the phase behavior of PEG, but the phase diagram of PNIPAM as reported by Afroze et al.[15] is qualitatively similar. Importantly, all of these models invoke a two-state assumption whereby the monomers interconvert between two forms. The models differ in the
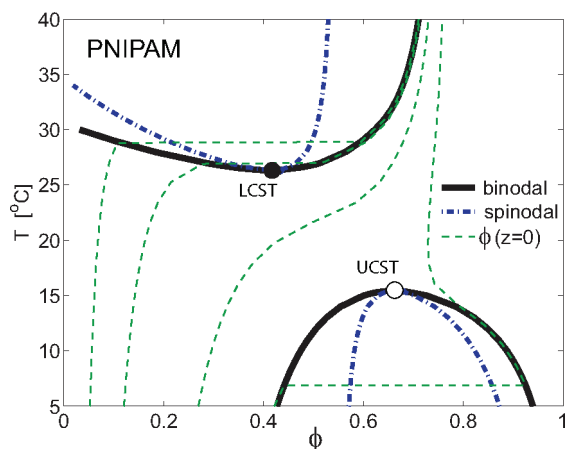
Figure 13. Phase diagram of PNIPAM depicting the binodals, spinodals and two critical points characterizing the LCST and UCST, as obtained from f_{int} of Afroze et al. (Appendix A2). In addition, the plot shows the volume fraction at the inner surface of the brush, $\phi(0)$ vs T, at $\sigma/p^{1/2}$ = 1/100, 1/30, 1/10, and 1/6 (from left to right). The "tie lines" in the $\phi(0)$ curves result from the onset of a vertical phase separation in the interior of the brush (see Figure 2 d−f).

identification of the interconverting monomeric states, polar vs. apolar, aggregated vs. non aggregated, H-bonded vs. non H-bonded etc. Roughly speaking one state is hydrophilic and the other is hydrophobic. The hydrophilic state is preferred at low T while the hydrophobic state is favored at high T. Implementing these models suggests that vertical phase separation in the brush gives rise to a hydrophilic exterior and a hydrophobic interior.[31] The two-state hypothesis, together with $\phi(z)$ allows to rationalize experimental results on wetting and aggregation. Two items illustrate this point. First is an early observation concerning the aggregation behavior of particles displaying PNIPAM brushes.[81] As T is raised to around 30°C the brush shrinks but without concurrent particle aggregation. Particle aggregation occurs only at higher T. Second is the observation of gradual decrease in brush thickness upon increasing of T but with an abrupt change in wetting angle occurring around 32 °C.[82] Both observations can be rationalized by the vertical phase separation scenario with the additional requirement that the outer dilute region is hydrophilic as suggested by two-state models.[31] This indirect support for the two-state models is supplemented by spectroscopic evidence for two interconverting monomeric states whose concentration ratio varies with T.[58]

We finally note two points: First the two-state models introduce a number of phenomenological parameters. Since most of these models concern the phase behavior of aqueous solutions of PEG, the model parameters were determined only for this system. Second, a recent two−state model[59] aimed specifically at rationalizing the PNIPAM phase diagram as reported by Rebelo et al.[43] by introducing cooperative hydration. However, this model predicts a "square-like" miscibility gap with a roughly horizontal binodal in contradiction to the experimental $\phi(z)$.

2. The f_{int} of Afroze et al.: Parameters, Virial Coefficients and Phase Diagram. The empirical f_{int} proposed by Afroze et al.[15] for PNIPAM is: $a^3 f_{int}(\phi) = (1 - \phi)\ln(1 - \phi) + \chi^{eff}(\phi,T)\cdot \phi(1 - \phi)$ with $\chi^{eff}(\phi,T) = - 12.947 + 0.044959T + 17.920\phi - 0.056944\phi T + 14.814\phi^2 - 0.051419\phi^2 T$, where T in this particular expression is a number which stands for temperature in units of Kelvin. For this PNIPAM model, $\hat{v} = 31.4\times(1-T/\Theta)$
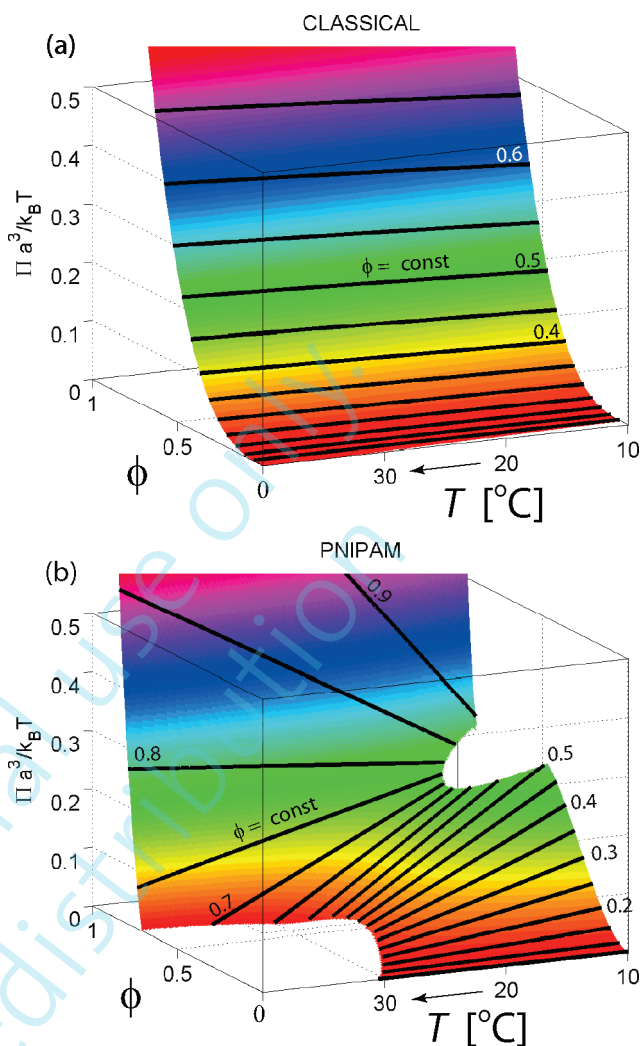

Figure 14. $\Pi a^3/k_B T$ vs ϕ and T for (a) classical (Θ = 34 °C) and (b) PNIPAM solutions in the range of 10 °C $\leq T \leq$ 40 °C. The black lines correspond to solutions of given ϕ. The classical iso-ϕ lines are weakly increasing with increasing T. The PNIPAM iso-ϕ lines exhibit much stronger variation with T and with a ϕ dependent slope. $\Pi a^3/k_B T$ at intermediate ϕ decreases with increasing T.

with Θ = 307.80K (34.66°C), and thus $\hat{v}$ decreases with increasing T. The third dimensionless virial coefficient is typically negative, $\hat{w} = -2.93 \times (1 - T/W)$ with W = 532.14 K, and thus close to -1 at $T = \Theta$. This model exhibits both a LCST and UCST with critical points at ϕ_c^{LCST} = 0.413, T_c^{LCST} = 299.510K (26.360 °C), and ϕ_c^{UCST} = 0.661, T_c^{UCST} = 288.546K (15.396 °C) (Fig. 13). The $\Pi(\phi,T) = \phi \partial f_{int}/\partial\phi - f_{int}$ predicted by the f_{int} of Afroze et al. differs qualitatively from the $\Pi(\phi,T)$ obtained from the classical $f_{int}a^3 = \hat{v}\phi^2 + \hat{w}\phi^3$. In the classical case $\Pi(\phi,T)$ slowly increases with T. In contrast, the $\Pi(\phi,T)$ obtained from f_{int} of Afroze et al. displays regions exhibiting the opposite trend and with much steeper T dependence (Figure 14)

Within this model, PNIPAM brushes exhibit collapse reminiscent of a classical brush under poor solvent conditions for $T \geq$ 30.5°C. They undergo vertical phase separation in the range $T_c^{LCST} \leq T \leq$ 30.5°C. At lower temperatures, down to $T = T_c^{UCST}$ the brush behavior is similar to that of classical brush under good solvent conditions. Vertical phase separation occurs again for $T \leq T_c^{UCST}$ but at high surface densities $\sigma/p^{1/2}$ (Fig. 13).

The model had been developed on the basis of experimental data in the range $10°C \leq T \leq 70°C$. To our knowledge there is currently no experimental evidence for the existence of the predicted UCST and we thus do not show results for the low T regime.

3. PNIPAM−Protein Interactions. The experimental study of PNIPAM−protein interactions is now emerging. The results suggest that the interactions between free PNIPAM chains and BSA are not purely repulsive. Fluorescence spectroscopy at pH = 7, $T = 25$ °C demonstrate that free PNIPAM chains can bind up to five proteins per chain.[61] While the precise number depends on concentrations and N this result suggests that BSA adsorbs onto the backbone of the chain rather than onto terminal groups. The interactions between BSA and PNIPAM brushes were also characterized by AFM with BSA coated tips at pH = 7.4 and $T = 22-34$ °C. There was no measurable adhesion below 25 °C and the adhesion force then increased with T reaching a plateau in the range $T = 29-34$ °C.[83] In contrast to the bulk results noted earlier, the AFM measurements suggest repulsive interactions below 25 °C. The PNIPAM monomer-protein interactions may vary with the protein species involved as indicated by studies of protein adsorption on brushes. These demonstrate strong effect of the swelling degree such that protein adsorption onto collapsed brushes is significantly higher. However, swollen brushes also adsorb proteins and the adsorbed species differ with the degree of swelling.[84,85]

4. Molecular Parameters of PNIPAM: a, p, and l_p. Modeling of PNIPAM brushes faces uncertainties concerning the chain structural parameters. The theoretical description of flexible chains is formulated in terms of persistent segments of length l_p and diameter a, corresponding to the size of a single monomer, such that $l_p \approx pa$. The literature values of these parameters vary widely. Xu et al.[86] estimate $a = 1.5$ Å while Zhu et al.[38] utilized $a = 3$ Å corresponding to two collinear C−C bonds. Malham and Bureau[37] estimated $a = 5$ Å utilizing $\Sigma H \approx Na^3$ and the data of Ishida and Biggs.[87] Ricka et al.[88] report a Kuhn length $l_K = 2pa \simeq 14-20$ Å, Bikert et al.[89] suggest $l_p \simeq 44$ Å while Zhang et al.[61] conclude $l_K = 2pa \approx 7$ Å as deduced from AFM force spectroscopy. Ahmed et al.[58] estimate $p \approx 10$ based on their analysis of the rate of collapse of PNIPAM chains. We are unaware of a report specifying simultaneously both a and l_p or addressing the possible T dependence of l_p. This last question is of interest in view of the suggestion that PNIPAM hydration is a cooperative process.[58,59] Results shown in the figures are obtained for $a = 5$ Å and $p = 1$.

APPENDIX B: THE INSERTION PENALTY WITHIN THE ALEXANDER MODEL

The direct evidence regarding the insertion scenario and eq 2 is from simulations studying the insertion of colloidal particles[22,25] and AFM tips[18,24] into brushes. The simulations reporting the concentration profiles demonstrate short ranged perturbation upon insertion of a small particle. The decay length is of order of few a. In addition, the insertion free energy in good solvents is consistent with an osmotic penalty for deeply inserted spheres[25] and for cylindrical AFM tips.[24] In the following we justify eq 1 by considering F_{ins} within the Alexander model focusing on a brush with immobile grafting sites. For this case we assume that the lateral perturbation of the monomer concentration profile is comparable in size to the cross section of the inserted particle as

suggested by simulations results. We thus analyze the case of a finite brush with a total area A_T comparable to the cross section of the inserted particle. In other words, the system considered corresponds to the brush region affected by the insertion induced perturbation. We argue that the effect of fully inserting a particle of volume V_{prt}^0 into a finite brush is 2-fold: (i) the brush height increases from H, its unperturbed value, to H_n; (ii) the volume available to the monomers of the A_T/Σ grafted chains is reduced from $A_T H_n$ to $A_T H_n - V_{prt}^0$. Accordingly Φ changes upon insertion of the particle from $\Phi = Na^3/H\Sigma$ to

$$\Phi_n = \frac{A_T}{\Sigma} \frac{Na^3}{A_T H_n - V_{prt}^0} = \frac{1}{y - Q} \Phi \tag{B1}$$

where $y = H_n/H \geq 1$ and $Q = V_{prt}^0/A_T H \ll 1$. For spherical particles of radius $R_{prt} \ll H$ such that $A_T \approx R_{prt}^2$ one obtains $Q \approx R_{prt}/H \ll 1$. In turn, $F_{ins} = A_T \Sigma^{-1}(F_{chain}^n - F_{chain})$ where F_{chain} and F_{chain}^n denote the free energies per chain before and after insertion. Altogether, the insertion penalty is

$$\frac{F_{ins}}{k_B T} = \frac{A_T}{\Sigma} \left[\frac{3}{2} \left(\frac{H_n^2 - H^2}{Npa^2} \right) + \frac{Nf_{int}(\Phi_n)a^3}{\Phi_n} - \frac{Nf_{int}(\Phi)a^3}{\Phi} \right] \tag{B2}$$

We expect H_n to increase with V_{prt}^0 and simultaneously $H_n \to H$ for $Q \to 0$. Accordingly we approximate $f_{int}(\Phi_n)$ by $f_{int}(\Phi_n) = f_{int}(\Phi) + (\partial f_{int}/\partial \Phi)|_\Phi (\Phi_n - \Phi)$ and y by $y = 1 + bQ$ where $b > 0$ is a constant depending on the solvent quality. Rewriting eq B2 using $\Phi = Na^3/H\Sigma$ and the equilibrium condition for the unperturbed brush, $\Pi a^3/k_B T = 3\sigma^2/\Phi$, yields

$$\frac{F_{ins}}{k_B T} = A_T H \left[\frac{(y^2 - 1)\Pi}{2k_B T} + (y - Q)f_{int}(\Phi_n) - f_{int}(\Phi) \right] \tag{B3}$$

Substituting $f_{int}(\Phi_n) = f_{int}(\Phi) + (\partial f_{int}/\partial \Phi)|_\Phi (\Phi_n - \Phi)$ leads to

$$\frac{F_{ins}}{k_B T} = \frac{A_T H}{k_B T} \left[\frac{\Pi}{2}(y^2 - 1) + \Pi(1 - y + Q) \right] \tag{B4}$$

Equation 5 is obtained upon substituting $y = 1 + bQ$ and neglecting terms containing Q^2. To determine b we begin with eq B3 and the equilibrium condition $\partial F_{ins}/\partial y = 0$ leading to

$$\frac{\Pi}{k_B T} y + f_{int}(\Phi_n) - \Phi_n \frac{\partial f_{int}(\Phi_n)}{\partial \Phi_n} = 0 \tag{B5}$$

Utilizing the method described earlier and the approximation $\partial f_{int}(\Phi_n)/\partial \Phi_n = \partial f_{int}(\Phi)/\partial \Phi + (\Phi_n - \Phi)\partial^2 f_{int}/\partial \Phi^2|_\Phi$ leads to

$$b = \frac{\Phi^2 \dfrac{\partial^2 f_{int}}{\partial \Phi^2}}{\dfrac{\Pi}{k_B T} + \Phi^2 \dfrac{\partial^2 f_{int}}{\partial \Phi^2}} \leq 1 \tag{B6}$$

APPENDIX C: THE SCF THEORY

The aim of this Appendix is to recall certain details of the SCF theory and obtain rigorous expressions for $\Pi(0)$ and $\bar{\Pi}$ for an arbitrary f_{int}. Within the version of the SCF theory we utilize,[13]

the free energy per chain in the brush is

$$\frac{F_{\text{chain}}}{k_B T} = \frac{F_{\text{el}}}{k_B T} + \frac{F_{\text{int}}}{k_B T}$$

$$= \frac{3}{2pa^2}\int_0^h \mathrm{d}x\, g(x) \int_0^x E(x,z)\,\mathrm{d}z + \Sigma\int_0^h f_{\text{int}}[\phi(z)]\,\mathrm{d}z \tag{C1}$$

The first term allows for the elastic free energy of a Gaussian chain while the second reflects the contribution due to monomer–monomer interactions. In the elastic free energy the length $E(x,z) = \mathrm{d}z/\mathrm{d}n$ is proportional to the local tension at z when the chain end is at x, $(3k_B T/pa^2)\, E(x,z)$, and n specifies the position of the monomer along the chain. $g(x)$ is the distribution function of the altitude of the free ends, x. The average tension per unit area at altitude z, $T_n(z)$, is thus

$$T_n(z) = \frac{3k_B T}{pa^2\Sigma}\int_z^h E(x,z)g(x)\,\mathrm{d}x \tag{C2}$$

The interaction free energy giving rise to the second term is specified in terms of a free energy density $k_B T f_{\text{int}}[\phi(z)]$. In the strong stretching approximation, only chains with $x \geq z$ contribute to $\phi(z)$ and the three unknown functions specifying the brush are related via

$$\phi(z) = \frac{a^3}{\Sigma}\int_z^h \frac{g(x)}{E(x,z)}\,\mathrm{d}x \tag{C3}$$

The brush properties are determined by minimization of F_{chain} subject to two constraints

$$\int_0^x \frac{\mathrm{d}z}{E(x,z)} = N \tag{C4a}$$

$$\frac{\Sigma}{a^3}\int_0^h \phi(z)\,\mathrm{d}z = N \tag{C4b}$$

The minimization of F_{chain} leads to two key equations

$$E(x,z) = \frac{\pi}{2N}\sqrt{x^2 - z^2} \tag{C5a}$$

$$\frac{a^3\partial f_{\text{int}}}{\partial\phi} \equiv U(\phi) = \Lambda - (\lambda z)^2, \quad \lambda^2 \equiv \frac{3\pi^2}{8pa^2N^2} \tag{C5b}$$

where $U(\phi) = \mu(\phi)/k_B T$ and $\mu(\phi)$ is the monomer exchange chemical potential (Appendix D). Once Λ is determined via the constraint C4b, this last equation allows to calculate $\phi(z)$ (Appendix D). We first utilize eqs C5 to obtain an explicit expression for $\Pi(z)$, eq 8, in terms of $\phi(z)$ for the yet unknown Λ and for an arbitrary f_{int}. This is then used to obtain eqs 9 and 12 for $\Pi(0)$ and $\bar{\Pi}$. To this end we introduce an elastic free energy density $k_B T f_{\text{el}}(z)$ such that $F_{\text{el}} = k_B T\Sigma\int f_{\text{el}}(z)\,\mathrm{d}z$ or

$$f_{\text{el}}(z) = \frac{3}{2pa^2\Sigma}\int_z^h E(x,z)g(x)\,\mathrm{d}x$$

$$= \frac{3\pi}{4Npa^2\Sigma}\int_z^h \sqrt{x^2 - z^2}g(x)\,\mathrm{d}x = \frac{T_n(z)}{2k_B T} \tag{C6}$$

allowing to specify $\mathrm{d}f_{\text{el}}(z)/\mathrm{d}z$ and obtain[34]

$$f_{\text{el}}(z) = -\int_z^h \frac{\mathrm{d}f_{\text{el}}}{\mathrm{d}z}\,\mathrm{d}z = \frac{\lambda^2}{a^3}\int_z^h t\phi(t)\,\mathrm{d}t \tag{C7}$$

Noting the similarity between the RHS of eq C7 and $\mathrm{d}U/\mathrm{d}z$ as given by eq C5b, together with $U(\phi) = a^3\partial f_{\text{int}}/\partial\phi$ and $\int_z^h U(\phi)\,\mathrm{d}\phi = \int_z^h \mathrm{d}f_{\text{int}}$ leads to[34]

$$\frac{2k_B T f_{\text{el}}(z)}{a^3} = \Pi(z) - \Pi(h) \tag{C8}$$

For a free brush at equilibrium, when $\Pi(h) = 0$, this ensures the local force balance, $\Pi(z) = T_n(z)$. It also specifies the local osmotic pressure within the SCF theory $\Pi(z)/k_B T = 2f_{\text{el}}(z)$, eq 8. Accordingly, $\Pi(0)$ as given by eq C7 and using $\langle z\rangle Na\sigma = \int_0^h z\phi(z)\,\mathrm{d}z$ leads to eq 9. The average osmotic pressure in the brush

$$\frac{\bar{\Pi}}{k_B T} = \frac{2}{h}\int_0^h f_{\text{el}}(z)\,\mathrm{d}z = \frac{2\lambda^2}{a^3 h}\int_0^h t\phi(t)\,\mathrm{d}t\int_0^t \mathrm{d}z$$

$$= \frac{2\lambda^2}{a^3 h}\int_0^h z^2\phi(z)\,\mathrm{d}z \tag{C9}$$

where the RHS is obtained upon changing the order of integration with respect to z and t. Since $\langle z^2\rangle Na\sigma = \int_0^h z^2\phi(z)\mathrm{d}z$ this leads to eq 12.

Our derivation of eqs 8, 9 and 12 invoked eq C5a for $E(x,z)$. Note however that these results can alternatively be obtained from eq 6, $\mu(\phi(z))/k_B T = \Lambda - (\lambda z)^2$, without solving for $E(x,z)$ since $\Pi(z)a^3/k_B T = \phi\mu/k_B T - a^3 f_{\text{int}}$ leads to

$$\frac{a^3 d\Pi(z)}{k_B T \mathrm{d}z} = \frac{\phi(z)}{k_B T}\frac{\partial\mu(\phi(z))}{\partial\phi}\frac{\partial\phi(z)}{\partial z} = -2\lambda^2 z\phi(z) \tag{C10}$$

upon utilizing $(\partial\mu/\partial\phi)(\partial\phi/\partial z) = -2\lambda^2 z$. This in turn leads to

$$\frac{a^3 \mathrm{d}\Pi(z)}{k_B T \mathrm{d}z} = \frac{\mathrm{d}}{\mathrm{d}z}\left(2\lambda^2\int_z^h t\phi(t)\,\mathrm{d}t\right) \tag{C11}$$

yielding eq 8 and leading also to eqs 9 and 12.

■ APPENDIX D: SOLVING THE SCF EQUATIONS

This appendix describes our algorithm to numerically solve the SCF equations and to obtain related results for arbitrary f_{int}, and a number of particle shapes. In particular, it allows one to reproduce the plots presented and create similar plots for user chosen parameters. To calculate the brush properties, we consider a smooth, otherwise arbitrary $f_{\text{int}}(\phi)$, defined for $0 \leq \phi \leq 1$ and which may exhibit non convex regions. In this last case the first step is to replace the non convex regions by a "tangent" specified by the Maxwell construction thus eliminating non stable regions from $f_{\text{int}}(\phi)$ and determining the phase diagram. The second step is the minimization of eq C1 subject to the constraints C4. This yields $\phi(z)$ and $\Pi(z)$. With this at hand it is straightforward to obtain $F_{\text{ins}}(z)$ and the different F_{att} as well as $c_{\text{prt}}(z)$ and the corresponding adsorption isotherms. For brevity we introduce a dimensionless interaction free energy density $f(\phi) \equiv a^3 f_{\text{int}}(\phi)$ and a dimensionless chemical potential $U(\phi) \equiv \mu/k_B T$ and denote the derivative of Y with respect to its argument, evaluated at x, by $Y'(x)$.

1. The Phase Diagram, $\mu(\phi)$ and $\phi_\pm$. In the Maxwell construction $U(\phi) = f'(\phi_\pm)$ in the coexistence region $\phi \in [\phi_-, \phi_+]$, and $U(\phi) = f'(\phi)$ outside this interval. To numerically obtain ϕ_- and ϕ_+, we aim to locate a ϕ^* corresponding to the middle intersection between a horizontal trial line and the van der Waals loop with the property $f'(\phi^*) = f'(\phi_\pm)$, where $\phi^* \in (\phi_-^S, \phi_+^S)$. This range is determined by two spinodal volume fractions $\phi_\pm^S$ fulfilling $f''(\phi_\pm^S) = 0$. To this end we introduce two functions,

$$I_-(\phi^*) \equiv \int_0^{\phi^*} \max(0, f'(\phi) - f'(\phi^*)) \, d\phi \tag{D1a}$$

$$I_+(\phi^*) \equiv \int_{\phi^*}^1 \max(0, f'(\phi) - f'(\phi^*)) \, d\phi \tag{D1b}$$

defining the net area $I_-(\phi^*) - I_+(\phi^*)$ bound between the horizontal $f'(\phi^*)$ and the curve $f'(\phi)$ within the interval $\phi \in [\phi_-, \phi_+]$. The proper ϕ^* is obtained by requiring the net area to vanish and $\phi_\pm$ are subsequently identified with the two solutions of $f'(\phi_\pm) = f'(\phi^*)$. Since $I_-(\phi_-^S) = I_+(\phi_+^S) = 0$, and $I_-(\phi_+^S) > 0$ and $I_+(\phi_-^S) > 0$, there is exactly one $\phi^* \in [\phi_-^S, \phi_+^S]$ with a vanishing net area. In the case of a classical brush under poor solvent conditions, $\phi_-^S = 0$ is set. With the monotonous $U(\phi)$ at hand, we have access to its inverse, the monotonous $U^{-1}(U)$. Overall, the algorithm described in this paragraph returns $\phi_\pm$, $\phi_\pm^S$ as well as the monotonous $U(\phi)$ and $U^{-1}(U)$.

2. The Lagrange Parameter Λ, $\phi(0)$ and the Brush Height h. Determining the Lagrange parameter, $\Lambda = U(\phi(0))$, amounts to finding the correct value for $\phi(0)$. To this end we scan through the range of values $\phi(0) \in [0,1]$, excluding the interval (ϕ_-, ϕ_+). For each attempted $\phi(0)$, we calculate an attempted brush height $h = [\Lambda - U(0)]^{1/2}/\lambda$, and numerically evaluate the integral $J \equiv \int_0^h U^{-1}(\Lambda - \lambda^2 z^2) \, dz$, using λ as defined in eq C5b. The procedure terminates when $J = Na\sigma$, in accord with constraint C4b. The values for h and $\phi(0)$ at termination are the equilibrium values characterize the solution of the SCF equations. An approximate analytical result for Λ, $\phi(0)$, h, and $\phi(z)$, perfectly matching the numerical results, is available for classical brushes in the full τ range.[34,51]

$\phi(z)$ and $\Pi(z)$ Profiles, the Free Ends Distribution $g(z)$ and The Free Energies F_{3l}, F_{int}. All remaining results are directly evaluated using the above quantities. The density profile is given by $\phi(z) = U^{-1}[\Lambda - (\lambda z)^2]$, the osmotic pressure is specified by $a^3\Pi(z)/k_BT = \phi(z)U(\phi(z)) - f(\phi(z))$ and the phase boundary is located at altitude $z_{co} = [\Lambda - U(\phi_+)]^{1/2}/\lambda$. In the absence of a phase boundary within the brush, ϕ_+ vanishes, and thus $z_{co} = h$, as it should. All profiles are evaluated at equidistantly spaced $z \in [0,h]$ upon direct insertion of z values into the available functions ϕ, U, f, and U^{-1}. The distribution of ends, $g(z)$, for which results are not shown within this manuscript, is calculated by means of the Abel transform. To be specific, when $\phi'(z)$ is continuous we evaluate

$$G(\eta) = -\eta \int_\eta^h \frac{\phi'(z) \, dz}{\sqrt{z^2 - \eta^2}} \tag{D2}$$

If $\phi'(z)$ is non-continuous at z_{co}, we ignore this point during the numerical integration. The corresponding integral, named $G_{co}(\eta)$, then evaluates easily for all η. We then add $G_{co}(\eta)$ to the analytical expression for the diverging contribution, $(\phi_+ - \phi_-)/(z_{co}^2 - \eta^2)^{1/2}$, arising from the step of $G_{co}(\eta)$, for all $\eta \leq z_{co}$; this

provides $G(\eta)$ for all η. The probability distribution $g(z)$ is obtained from $G(\eta)$ by subsequent normalization, $g(z) = G(z)/Z$ with the constant $Z \equiv \int_0^h G_{co}(\eta) \, d\eta + \pi(\phi_+ - \phi_-)/2$ so that the discontinuity is numerically integrated out exactly. There is thus no need to employ a $Z = Na\sigma$ relationship, as it becomes an approximation in a numerical implementation. In the absence of any discontinuity, $\phi_\pm = 0$ and $G_{co} = G$. It is straightforward to evaluate the equilibrium free energy F_{chain} and its two contributing terms, F_{int} and F_{el}. To this end it is however useful to notice that F_{el}, as given by eq C5a, simplifies to $F_{el}/k_BT = (1N\lambda^2/2)\int_0^h z^2 g(z) \, dz = N\lambda^2 \langle z^2 \rangle/2$.

4. $F_{ins}(z)$, $F_{att}(z)$, and the Particle Concentration Profile $c_{prt}(z)$. To evaluate $F_{int}(z)$ and $F_{att}(z)$ defined by eqs 1 and 24 we need expressions for the infinitesimal area $A_{prt}(z,z')$ and the circumference $S_{prt}(z,z')$ at z' for particles of given shape, whose geometric centers are located at $z > 0$. In the limit of infinitely small particles, $A_{prt}(z,z') = V_{prt}^0 \delta(z - z')$ and $S_{prt}(z,z') = A_{prt}^0 \delta(z - z')$. More generally, it is useful to introduce the distance between the particle's center and the brush altitude, $z' = z + \Delta z$, such that $A_{prt}(z,z')$ and $S_{prt}(z,z')$ both vanish if (i) $2|\Delta z|$ exceeds the vertical extension, $L_|$, of the inserted particle, or (ii) $z < L_|$, reflecting the impenetrability of the wall. The following discussion concerns the remaining z and z'.

BSA is modeled as equilateral triangular wedge[90] with edges of length $L_E = 80$ Å, maximal horizontal extension (thickness) $L_- = 30$ Å, and maximal vertical extension $L_| = (L_E^2 - (L_E/2)^2)^{1/2} \approx 69.3$ Å. Making use of the step function $\mathscr{H}(x > 0) \equiv L_|L_-$ and $\mathscr{H}(x \leq 0) \equiv 0$, such a shape is characterized by

$$A_{BSA}(z,z') = \frac{(L_| \pm 2\Delta z)L_-}{\sqrt{3}}$$

$$S_{BSA}(z,z') = \frac{2\left[L_| + 2L_- \pm 2\Delta z + \mathscr{H}\left(\pm \Delta z - \frac{1}{2}L_|\right)\right]}{\sqrt{3}} \tag{D3}$$

capturing the cases of ∇- and Δ-oriented wedges. The former, employing the positive sign, has its apex facing the grafting surface. The two sets of expressions lead to $(3)^{1/2}A_{BSA} = 2(L_| + 3L_-)L_| = L_E(3L_- + L_|) \approx 1.27 \times 10^4$ Å^2 and $(3)^{1/2}V_{BSA}^0 = L_-(L_|)^2 = L_|L_-L_E/2 \approx 8.3 \times 10^4$ Å^3. For spherical particles of radius $R = L_|/2$,

$$A_\circ(z,z') = \pi(R^2 - \Delta z^2),$$
$$S_\circ(z,z') = \pi L_| \tag{D4}$$

thus leading to the correct $A_\circ^0 = 4\pi R^2$ and $V_\circ^0 = (\pi/6)(L_|)^3$. A sphere with BSA volume has diameter 54.1 Å.

Inserting eqs D3 and D4 into eqs 1 and 24 we obtain $F_{ins}(z)$ and the ternary adsorption $F_{att}(z)$ thus determining the corresponding particle concentration profiles $c_{prt}(z)$ and the related $\Gamma = \int_0^h c_{prt}(z) \, dz$ for both fully and partially inserted particles. The cases of primary and ligand adsorption are special cases modeled by setting $z = L_|/2$ and $z = z_L > L_|/2$, respectively, while using a constant $F_{att}(z)$ instead of eq 24.

■ AUTHOR INFORMATION

Corresponding Author

*E-mail: (A.H.) avraham.halperin@ujf-grenoble.fr; (M.K.) mk@mat.ethz.ch.

■ REFERENCES

(1) Elbert, D. L.; Hubbell, J. A. *Annu. Rev. Mater. Sci.* **1996**, *26*, 365–394.

(2) Lee, H. J.; Lee, H. B.; Andrade, J. D. *Prog. Polym. Sci.* **1995**, *20*, 1043.

(3) (a) Harris, J. M., Ed. *Poly(ethylene glycol) Chemistry: Biotechnical and Biomedical Applications*; Plenum Press: New York, 1992; (b) Harris, J. M., Zalipsky, S., Eds. *Poly(ethylene glycol) Chemistry and Biological Applications*; American Chemical Society: Washington DC, 1997.

(4) Cole, M. A.; Voelcker, N. H.; Thissen, H.; Griesser, H. J. *Biomater.* **2009**, *30*, 1827.

(5) Yoshizako, K.; Akiyama, Y.; Yamanaka, H.; Shinohara, Y.; Hasegawa, Y.; Carredano, E.; Kikuchi, A.; Okano, T. *Anal. Chem.* **2002**, *74*, 4160.

(6) Kikuchi, A.; Okano, T. *Prog. Polym. Sci.* **2002**, *27*, 1165.

(7) Huber, D. L.; Samara, M. A.; Kim, B.-I.; Bunker, B. *Science* **2003**, *301*, 352.

(8) Yamada, N.; Okano, T.; Sakai, H.; Karikusa, F.; Sawasaki, Y.; Sakurai, Y. *Makromol. Chem. Rapid Commun.* **1990**, *11*, 571.

(9) da Silva, R. M. P.; Mano, J. F.; Reis, R. L. *Trends Biotechnol.* **2007**, *25*, 577.

(10) Yang, J.; Yamato, M.; Okano, T. *MRS Bull.* **2005**, *30*, 189.

(11) Cooperstein, M. A.; Canavan, H. E. *Langmuir* **2010**, *26*, 7695.

(12) Milner, S. T.; Witten, T. A.; Cates, M. E. *Macromolecules* **1988**, *21*, 2610.

(13) Zhulina, E. B.; Borisov, O. V.; Priamitsyn, V. A. *J. Colloid Interface Sci.* **1990**, *137*, 495.

(14) Milner, S. T. *Science* **1991**, *251*, 905.

(15) Afroze, F.; Nies, E.; Berghmans, H. *J. Mol. Struct.* **2000**, *554*, 55.

(16) (a) Yim, H.; Kent, M. S.; Satija, S.; Mendez, S.; Balamurugan, S. S.; Balamurugan, S.; Lopez, G. P. *Phys. Rev. E* **2005**, *72*, 051801. (b) Yim, H.; Kent, M. S.; Mendez, S.; Lopez, G. P.; Satija, S.; Seo, Y. *Macromolecules* **2006**, *39*, 3420.

(17) Koga, T.; Tanaka, F.; Motokawa, R.; Koizumi, S.; Winnik, F. M. *Macromolecules* **2008**, *41*, 9413.

(18) Murat, M.; Grest, G. S. *Macromolecules* **1996**, *29*, 8282.

(19) Halperin, A. *Langmuir* **1999**, *15*, 2525.

(20) Steels, B. M.; Koska, J.; Haynes, C. A. *J. Chromatogr. B* **2000**, *743*, 41.

(21) Halperin, A.; Fragneto, G.; Schollier, A.; Sferrazza, M. *Langmuir* **2007**, *23*, 10603.

(22) Milchev, A.; Dimitrov, D. I.; Binder, K. *Polymer* **2008**, *49*, 3611.

(23) Halperin, A.; Kröger, M. *Langmuir* **2009**, *25*, 11621.

(24) Halperin, A.; Zhulina, E. B. *Langmuir* **2010**, *26*, 8933.

(25) Ermilov, V.; Lazutin, A.; Halperin, A. *Macromolecules* **2010**, *43*, 3511.

(26) de Gennes, P.-G. *Scaling Concepts in Polymer Physics*; Cornell, University Press: Ithaca, NY, 1979.

(27) Grosberg, A. Yu.; Khokhlov, A. R. *Statistical Physics of Macromolecules*; American Institute of Physics: New York, 1994.

(28) Wagner, M.; Brochard Wyart, F.; Hervet, H.; de Gennes, P.—G. *Colloid Polym. Sci.* **1993**, *271*, 621.

(29) Halperin, A. *Eur. Phys. J. B* **1998**, *3*, 359.

(30) Baulin, V. A.; Halperin, A. *Macromol. Theory Simul.* **2003**, *12*, 549.

(31) Baulin, V. A.; Zhulina, E. B.; Halperin, A. *J. Chem. Phys.* **2003**, *119*, 10977.

(32) Toomey, R.; Tirrell, M. *Annu. Rev. Phys. Chem.* **2008**, *59*, 493.

(33) Karim, A.; Satija, S. K.; Douglas, J. F.; Ankner, J. F.; Fetters, L. J. *Phys. Rev. Lett.* **1994**, *73*, 3407.

(34) Halperin, A.; Kröger, M.; Zhulina, E. B. *Macromolecules* **2011**, *44*, 3622.

(35) Kubota, K.; Fujishige, S.; Ando, I. *J. Phys. Chem.* **1990**, *94*, 5154.

(36) Wang, X.; Qiu, X.; Wu, C. *Macromolecules* **1998**, *31*, 2972.

(37) Malham, I. B.; Bureau, L. *Langmuir* **2010**, *26*, 4762.

(38) Zhu, X.; Yan, C.; Winnik, F. M.; Leckband, D. *Langmuir* **2007**, *23*, 162.

(39) Cohen, J. A.; Podgornik, R.; Hansen, P. L.; Parsegian, V. A. *J. Phys. Chem. B* **2009**, *113*, 3709.

(40) Heskins, M.; Guillet, J. E. *J. Macromol. Sci.—Chem. A* **1968**, *2*, 1441.

(41) Fujishinge, S.; Kubota, K.; Ando, I. *J. Phys. Chem.* **1989**, *93*, 3311.

(42) Schild, H. G.; Tirrell, D. A. *J. Phys. Chem.* **1990**, *94*, 4352.

(43) (a) Gomes de Azevedo, R.; Rebelo, L. P. N.; Ramos, A. M.; Szydlowski, J.; de Sousa, H. C.; Klein, J. *Fluid Phase Equilib.* **2001**, *185*, 189. (b) Rebelo, L. P. N.; Visak, Z. P.; de Sousa, H. C.; Szydlowski, J.; Gomes de Azevedo, R.; Ramos, A. M.; Najdanovic-Viask, V.; Nunes da Ponte, M.; Klein, J. *Macromolecules* **2002**, *35*, 1887.

(44) (a) Jeon, S. I.; Lee, J. H.; Andrade, J. D.; de Gennes, P.-G. *J. Colloid Interface Sci.* **1991**, *142*, 149.

(45) Szleifer, I. *Biophys. J.* **1997**, *72*, 595.

(46) Currie, E. P. K.; Van der Gucht, J.; Borisov, O. V.; Cohen Stuart, M. A. *Pure Appl. Chem.* **1999**, *71*, 1227.

(47) Currie, E. P. K.; Norde, W.; Cohen Stuart, M. A. *Adv. Colloid Sci.* **2003**, *100—102*, 205.

(48) Yin, Z.; Zhang, J.; Jiang, L.-P.; Zhu, J.-J. *J. Phys. Chem. C* **2009**, *113*, 16104.

(49) Alexander, S. *J. Phys. (Paris)* **1977**, *38*, 977.

(50) Louis, A. A.; Bolhuis, P. G.; Meijer, E. J.; Hansen, J. P. *J. Chem. Phys.* **2002**, *116*, 10547.

(51) Software solving the SCF equations for classical and PNIPAM brushes with user set parameters is available at http://www.complex-fluids.ethz.ch.

(52) Mendez, S.; Curro, J. G.; McCoy, J. D.; Lopez, G. P. *Macromolecules* **2005**, *38*, 174.

(53) Dockal, M.; Carter, D. C.; Rüker, F. *J. Biol. Chem.* **1999**, *41*, 29303 and references therein.

(54) M, Carter, D. C.; Rüker, F. *J. Biol. Chem.* **1999**, *41*, 29303 and references cited therein.

(55) (a) Baskir, J. N.; Hatton, T. A.; Suter, U. W. *Macromolecules* **1987**, *20*, 1300. (b) Baskir, J. N.; Hatton, T. A.; Suter, U. W. *J. Phys. Chem.* **1989**, *93*, 2111. (c) Abbott, N. L.; Blankschtein, D.; Hatton, T. A. *Macromolecules* **1992**, *24*, 4334. (d) Abbott, N. L.; Blankschtein, D.; Hatton, T. A. *Macromolecules* **1992**, *25*, 3917. (e) Abbott, N. L.; Blankschtein, D.; Hatton, T. A. *Macromolecules* **1992**, *25*, 3932.

(56) The chemical potential of component i is specified in terms of dimensionless activity $a_i = \gamma_i c_i / c_i^\circ$ where c_i is the molar concentration, $c_i^\circ = 1$ mol/liter corresponding to a hypothetical standard state exhibiting Henry's law and γ_i is an activity coefficient such that $\gamma_i \rightarrow 1$ when $c_i \rightarrow 0$.[57] Accordingly, the numerical value of a_i for a dilute solution is identical to the dimensionless value of the molar c_i. To simplify the notation we thus denote the activity by the corresponding c_i.

(57) *International Union of Pure and Applied Chemistry: Quantities, Units and Symbols in Physical Chemistry*, 2nd ed.; Blackwell Science: Oxford, U.K.; 1993 available at http://www.iupac.org/publications/books/gbook/green_book_2ed.pdf.

(58) Ahmed, Z.; Gooding, E. A.; Pimenov, K. V.; Wang, L.; Asher, S. A. *J. Phys. Chem B* **2009**, *113*, 4248.

(59) Okada, Y.; Tanaka, F. *Macromolecules* **2005**, *38*, 4465.

(60) For preliminary results see: Schollier, A.; Frangneto., G.; Halperin. A.; Sferraza, M. ILL report 9—13—197 (2007) available at http://club.ill.fr/cv/servlet/ReportFind.

(61) Zhang, L.; Wu, B.; Su, Z.; Chen, X. *Polymer* **2008**, *49*, 5622.

(62) Cocke, D. L.; Wang, H. J.; Chen, J. *J. Chem. Commun.* **1997**, *23*, 2331.

(63) Becker, A.; Schlichting, I.; Kabsch, W.; Schultz, S.; Wagner, A. F. V. *J. Biol. Chem.* **1998**, *273*, 11413.

(64) Kim, J. U.; O'Shaughnessy, B. *Macromolecules* **2006**, *39*, 413–425.

(65) Yaneva, J.; Dimitrov, D. I.; Milchev, A.; Binder, K. *J. Colloid Interface Sci.* **2009**, *336*, 51.

(66) (a) Tamai, Y.; Tanaka, H.; Nakanishi, K. *Macromolecules* **1996**, *29*, 6750. (b) Tamai, Y.; Tanaka, H.; Nakanishi, K. *Macromolecules* **1996**, *29*, 6761.

(67) Longhi, G.; Lebon, F.; Abbate, S.; Fornili, S. I. *Chem. Phys. Lett.* **2004**, *386*, 123.

(68) Walter, J.; Deublein, S.; Vrabec, J.; Hasse, H. In *High Performance Computing in Science and Engineering*; Nagel, W. E., Kroher, D. B., Resch, M. M., Eds.; Springer: Berlin, 2010.

(69) Schuld, N.; Wolf, B. A. *Polymer Handbook*, 4th ed; Wiley: New York, 1999.

(70) (a) de Gennes, P.-G. *C. R. Acad. Sci, Paris II* **1991**, *117*, 313. (b) de Gennes, P.-G. *Simple Views on Condensed Matter*; World Scientific: Singapore, 1992.

(71) Šolc, K.; Dušek., K.; Koningsveld, R.; Berghmans, H. *Collect. Czech. Chem. Commun.* **1995**, *60*, 1661.

(72) Zhou, X.; Li, J.; Wu, C.; Zheng, B. *Macromol. Rapid Commun.* **2008**, *29*, 1363.

(73) Goldstein, R. *J. Chem. Phys.* **1984**, *80*, 5340.

(74) Karlstrӧöm, G. *J. Phys. Chem.* **1985**, *89*, 4962.

(75) Matsuyama, A.; Tanaka, F. *Phys. Rev. Lett.* **1990**, *65*, 341.

(76) Veytsman, B. A. *J. Phys. Chem.* **1990**, *94*, 8499.

(77) de Gennes, P.-G. *C. R. Acad. Sci., Ser. II* **1991**, *313*, 1117.

(78) Bekiranov, S.; Bruinsma, R.; Pincus, P. *Europhys. Lett.* **1993**, *24*, 183.

(79) Bekiranov, S.; Bruinsma, R.; Pincus, P. *Phys. Rev. E* **1997**, *55*, 577.

(80) Dormidontova, E. *Macromolecules* **2002**, *35*, 987.

(81) (a) Zhu, P. W.; Napper, D. H. *J. Colloid Interface Sci.* **1994**, *164*, 489. (b) Zhu, P. W.; Napper, D. H. *Coll. Surf. A* **1996**, *113*, 145.

(82) Balamurugan, S.; Mendez, S. S.; Balamurugan, M. J.; Brien, O., II; Lopez, G. P. *Langmuir* **2003**, *19*, 2545.

(83) (a) Cho, E.-C.; Kim, Y. D.; Cho, K. *J. Colloid Interface Sci.* **2004**, *286*, 479. (b) Cho, E.-C.; Kim, Y. D.; Cho, K. *Polymer* **2004**, *45*, 3195.

(84) Yu, Q.; Zhang, Y.; Chen, H.; Wu, Z.; Huang, H.; Chen, C. *Coll. Surf. B: Biointerfaces* **2010**, *76*, 468.

(85) Janzen, J.; Le, Y.; Kizhakkedathu, J. N.; Brooks, D. E. *J. Biomater. Sci. Polym. Edn.* **2004**, *15*, 1121.

(86) Xu, J.; Zhu, Z.; Luo, S.; Wu, C.; Lin., S. *Phys. Rev. Lett.* **2006**, *96*, 027802.

(87) Ishida, N.; Biggs, S. *Langmuir* **2007**, *23*, 11083.

(88) Ricka, J.; Gysel, H.; Schneider, J.; Nyffenegger, R.; Binkert, T. *Macromolecules* **1987**, *20*, 1407.

(89) Binkert, T.; Oberreich, J.; Meewes, M.; Nyffenegger, R.; Ricka, J. *Macromolecules* **1991**, *24*, 5806.

(90) Carter, D. C.; Ho, J. X. *Adv. Protein Chem.* **1994**, *45*, 153.